Article

Placenta-tropic VEGF mRNA lipid nanoparticles ameliorate murine pre-eclampsia

https://doi.org/10.1038/s41586-024-08291-2

Received: 18 September 2023

Accepted: 25 October 2024

Published online: 11 December 2024

Check for updates

Kelsey L. Swingle[1], Alex G. Hamilton[1], Hannah C. Safford[1], Hannah C. Geisler[1], Ajay S. Thatte[1], Rohan Palanki[1], Amanda M. Murray[1], Emily L. Han[1], Alvin J. Mukalel[1], Xuexiang Han[1], Ryann A. Joseph[1], Aditi A. Ghalsasi[1], Mohamad-Gabriel Alameh[2,3], Drew Weissman[2,3] & Michael J. Mitchell[1,3,4,5,6,7]✉

Pre-eclampsia is a placental disorder that affects 3–5% of all pregnancies and is a leading cause of maternal and fetal morbidity worldwide[1,2]. With no drug available to slow disease progression, engineering ionizable lipid nanoparticles (LNPs) for extrahepatic messenger RNA (mRNA) delivery to the placenta is an attractive therapeutic option for pre-eclampsia. Here we use high-throughput screening to evaluate a library of 98 LNP formulations in vivo and identify a placenta-tropic LNP (LNP 55) that mediates more than 100-fold greater mRNA delivery to the placenta in pregnant mice than a formulation based on the Food and Drug Administration-approved Onpattro LNP (DLin-MC3-DMA)[3]. We propose an endogenous targeting mechanism based on β_2-glycoprotein I adsorption that enables LNP delivery to the placenta. In both inflammation- and hypoxia-induced models of pre-eclampsia, a single administration of LNP 55 encapsulating vascular endothelial growth factor (VEGF) mRNA resolves maternal hypertension until the end of gestation. In addition, with our VEGF mRNA LNP 55 therapeutic, we demonstrate improvements in fetal health and partially restore placental vasculature, the local and systemic immune landscape and serum levels of soluble Fms-like tyrosine kinase-1, a clinical biomarker of pre-eclampsia[1]. Together, these results demonstrate the potential of this mRNA LNP platform for treating placental disorders such as pre-eclampsia.

Pre-eclampsia affects 3–5% of all pregnancies and is characterized clinically by gestational hypertension, sometimes accompanied by proteinuria, kidney and liver injury, neurological conditions including seizures, or fetal growth restriction[1]. The pathogenesis of pre-eclampsia is frequently described by a two-stage paradigm of placental dysfunction[1,4]. In normal pregnancy, extravillous trophoblasts from the placenta invade the uterine myometrium, remodelling and dilating the spiral arteries to create a low-resistance, high-blood-flow environment at the chorionic villi (maternal–fetal interface)[1,2]. The first stage of pre-eclampsia is caused by impaired spiral artery remodelling, creating a high-velocity and turbulent blood flow environment that results in the second stage of pre-eclampsia: placental hypoxia and oxidative stress[1]. This damage to the placenta induces abnormal secretion of antiangiogenic factors such as soluble Fms-like tyrosine kinase-1 (sFlt-1), which is believed to drive disease progression and hypertension[1]. Placenta-derived sFlt-1 is upregulated during pre-eclampsia and sequesters vascular endothelial growth factor (VEGF), hindering vasodilation.

No therapeutic has been clinically approved to slow pre-eclampsia progression; rather, the only curative option is delivery of the placenta and fetus[1]. Treatment plans include managing delivery until more advanced gestation is achieved while prescribing medications to manage blood pressure, prevent seizures and promote fetal lung maturity[1]. To this end, groups have sought to develop therapeutics that address the underlying placental dysfunction associated with pre-eclampsia. Preclinical research efforts include recombinant VEGF therapeutics[5–7], viral-vector-mediated overexpression of VEGF through systemic and local administration approaches[8–12], and gene silencing technologies using small interfering RNAs (siRNAs) to knock down sFlt-1 (refs. 13,14). Although these approaches have shown some preclinical success, recombinant proteins and siRNA conjugates have pharmacokinetic and local delivery limitations, whereas viral-vector-based gene therapy faces several challenges including immunogenicity, non-specific delivery, and packaging and manufacturing limitations[15,16].

Recently, ionizable lipid nanoparticles (LNPs) have demonstrated tremendous clinical success as a non-viral platform for nucleic acid delivery, with the Food and Drug Administration approval of the Onpattro siRNA therapeutic for hereditary transthyretin-mediated amyloidosis (hATTR) in 2018 and the Pfizer/BioNTech and Moderna COVID-19 messenger RNA (mRNA) vaccines a few years later[3,17,18]. Upon intravenous (i.v.) administration, LNPs traditionally deliver their cargo to the liver through a pathway based on apolipoprotein E (ApoE) adsorption; thus, early clinical applications of LNP therapeutics were limited

[1]Department of Bioengineering, University of Pennsylvania, Philadelphia, PA, USA. [2]Department of Medicine, University of Pennsylvania, Philadelphia, PA, USA. [3]Penn Institute for RNA Innovation, Perelman School of Medicine, Philadelphia, PA, USA. [4]Abramson Cancer Center, Perelman School of Medicine, University of Pennsylvania, Philadelphia, PA, USA. [5]Institute for Immunology, Perelman School of Medicine, University of Pennsylvania, Philadelphia, PA, USA. [6]Cardiovascular Institute, Perelman School of Medicine, University of Pennsylvania, Philadelphia, PA, USA. [7]Institute for Regenerative Medicine, Perelman School of Medicine, University of Pennsylvania, Philadelphia, PA, USA. ✉e-mail: mjmitch@seas.upenn.edu

to liver-centric diseases[19–21]. Recent preclinical efforts have focused on extrahepatic LNP delivery to broaden the application of LNPs to include disorders originating outside the liver[20–22], including previous work by our laboratory and others to develop LNPs for extrahepatic mRNA delivery to the placenta[23–27]. These works employed typical in vitro screening approaches to identify lead LNP candidates for placental mRNA delivery. However, in vitro LNP delivery can be poorly predictive of in vivo fate, making it difficult to rationally design LNP libraries on the basis of in vitro performance[28]. To overcome this challenge, high-throughput LNP barcoding has been used as an in vivo screening approach, enabling evaluation of large libraries of LNPs in more complex biological environments using DNA barcodes (b-DNAs)[28–31].

Here we report the use of a high-throughput screening approach using b-DNAs to engineer an mRNA LNP platform for the treatment of pre-eclampsia (Fig. 1a). From a library of 98 LNP formulations, we identified a placenta-tropic formulation (LNP 55) that enabled more than an order of magnitude greater luciferase mRNA delivery to the placenta than the industry standard C12-200 and clinical standard DLin-MC3-DMA LNPs[32–34]. We propose a potential protein-adsorption-based endogenous targeting mechanism that could promote delivery to the placenta. In an inflammation-induced mouse model of pre-eclampsia, we observed greater LNP 55 delivery to placental immune cells in diseased mice compared with healthy pregnant mice. Finally, through a single injection of placenta-tropic LNPs encapsulating VEGF mRNA, we were able to rescue maternal hypertension until the end of gestation in both inflammation- and hypoxia-induced models of pre-eclampsia. Together, these results demonstrate the potential of this LNP platform for mRNA delivery to the placenta to treat pre-eclampsia and other placental disorders during pregnancy.

High-throughput in vivo LNP screening

Achieving extrahepatic delivery to limit LNP-mediated liver toxicity is particularly important for the treatment of pre-eclampsia, as HELLP syndrome (haemolysis, elevated liver enzymes and low platelets) is often observed in patients with severe pre-eclampsia[35]. Studies have used various approaches to achieve extrahepatic LNP delivery, including designing new ionizable lipids[36,37], altering the excipient composition[38–40], adding permanently charged moleculues[20–22] and functionalizing the surface with active targeting moieties[41–44]. Here we designed a 98-LNP library with 24 unique ionizable lipids synthesized through S_N2 reaction chemistry from eight polyamine cores and three alkyl epoxides[32] (Extended Data Fig. 1a and Supplementary Figs. 1 and 2). For the remaining LNPs in the library, 12 of the ionizable lipids were further explored by varying excipient composition (Extended Data Fig. 1a and Supplementary Table 1). The industry standard C12-200 ionizable lipid for mRNA delivery and the clinically approved DLin-MC3-DMA ionizable lipid from Onpattro were also included as liver-tropic LNP controls[3,32,45]. A lipid phase containing ionizable lipid, phospholipid, cholesterol and lipid-poly(ethylene glycol) (PEG) was prepared for each LNP in the library (Table S1) to encapsulate a unique 61 nucleotide b-DNA (Extended Data Fig. 1b and Supplementary Table 2). Physicochemical characteristics of LNPs, including z-average diameter, polydispersity index, surface zeta potential, and encapsulation efficiency, were then evaluated (Supplementary Fig. 3 and Supplementary Table 3).

All 98 LNPs were pooled and administered i.v. to non-pregnant and pregnant mice (Extended Data Fig. 1b). Six hours after administration, mice were euthanized, and the heart, lungs, liver, kidneys, spleen, uterus, placentas and fetuses were collected. To assess whether LNP delivery to the placentas and fetuses varied according to location in the uterine horn[46,47], we distinguished proximal placentas and fetuses that were located closest to the ovaries from distal placentas and fetuses located closest to the cervix (Supplementary Fig. 4). Tissues were processed to extract b-DNA for detection of LNP delivery using next-generation sequencing (Extended Data Fig. 1b). LNP delivery to tissues in non-pregnant (Extended Data Fig. 1c) and pregnant mice (Fig. 1b) was visualized using heatmaps.

Using these high-throughput screening results, we aimed to determine the effects of changing the ionizable lipid and excipient formulation on LNP delivery (Supplementary Figs. 5 and 6). Of the polyamine cores used for ionizable lipid synthesis, several enabled extrahepatic LNP delivery, including the 480, 482, 488, 494 and 497 cores for delivery to the placentas (Supplementary Fig. 5). Notably, LNPs containing ionizable lipids with 16-carbon alkyl tails demonstrated greater accumulation in most tissues than those containing lipids with 12-carbon tails, despite having lower encapsulation efficiencies (Supplementary Figs. 3g and 5). These results could perhaps be explained by the enhanced stability conferred by the longer alkyl chains, but the lower encapsulation efficiencies of these LNPs limit their utility for potent mRNA transfection. To further examine the potential for extrahepatic LNP delivery, we performed enrichment analysis and constructed volcano plots to identify LNPs that were either significantly depleted (top left quadrant) or significantly enriched (top right quadrant) in a particular tissue compared with the C12-200 LNP formulation (Extended Data Fig. 2a–c). Unsurprisingly, as the C12-200 LNP demonstrated strong liver tropism, 41 and 12 of our LNP formulations were depleted relative to C12-200 in the livers of non-pregnant and pregnant mice, respectively. Encouragingly, 52 LNPs mediated significantly greater delivery to the distal placentas compared with the C12-200 formulation.

To understand the relationship between hepatic and extrahepatic delivery, we calculated the correlation coefficient of normalized delivery between each tissue pair (Extended Data Fig. 2d–g). In both non-pregnant and pregnant mice, LNP delivery to the liver demonstrated weak correlation with delivery to the extrahepatic organs; however, delivery to a given extrahepatic organ was generally strongly correlated with delivery to another extrahepatic organ (Extended Data Fig. 2d–e). Delivery to the placentas and fetuses was weakly correlated with delivery to the other maternal tissues (Extended Data Fig. 2g). The correlation of normalized delivery between distal and proximal placentas as well as distal and proximal fetuses was very strong, with squared correlation coefficients of 0.978 and 0.845, respectively (Extended Data Fig. 2g and Supplementary Fig. 7). These results indicate that the location of a placenta or fetus in the uterine horn may not affect LNP delivery.

Validation of a placenta-tropic mRNA LNP

We next sought to validate the high-throughput screening results from our pooled library by individually evaluating LNP formulations and their ability to deliver luciferase mRNA in vivo. As it is important to validate the use of high-throughput screening to identify both hits and poorly performing LNPs, we selected LNP 6, which ranked at the fifth percentile for delivery to the lungs, liver, spleen and placentas, as a negative control (Supplementary Fig. 8). To select our placenta-tropic LNP formulation, we used least-squares linear regression on encapsulation efficiency or normalized b-DNA delivery to the placenta using LNP formulation parameters (ionizable lipid structure and excipient composition) as explanatory variables (Supplementary Tables 4–8). Although the 480, 482 and 488 polyamine cores and C16 epoxide tails contributed positively to placental delivery, their capacity for generating formulations with high encapsulation efficiencies seemed to be limited, leading us to select the C14-494 ionizable lipid. Ultimately, we selected LNP 55 as our placenta-tropic formulation, as it contained a greater amount of the 1,2-dioleoyl-*sn*-glycero-3-phosphoethanolamine (DOPE) phospholipid that was identified through regression analysis as a key parameter influencing proximal and distal placental delivery. Finally, we selected standard LNPs 97 (C12-200) and 98 (DLin-MC3-DMA), which demonstrated potent delivery to the liver with minimal placental delivery in our high-throughput screen (Supplementary Fig. 8).

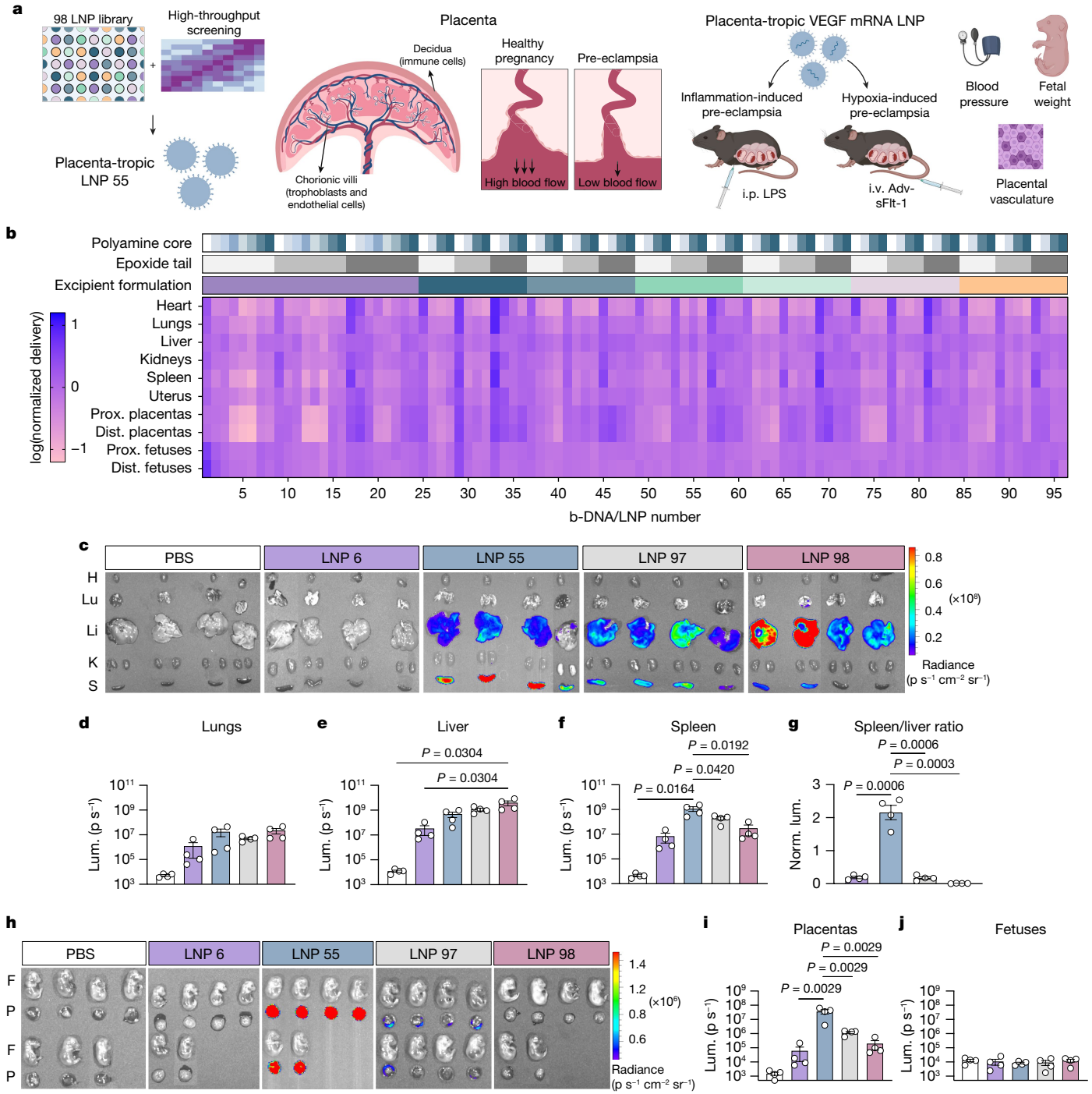

Fig. 1 | High-throughput in vivo screening to identify a placenta-tropic LNP formulation for the treatment of pre-eclampsia. a, High-throughput in vivo screening was employed to identify a placenta-tropic formulation LNP 55 from a library of 98 LNP formulations. LNP 55 was used to deliver therapeutic VEGF mRNA in inflammation- and hypoxia-induced murine models of pre-eclampsia. **b**, Using a high-throughput in vivo screening approach, 98 LNP formulations encapsulating a unique b-DNA cargo were pooled and administered i.v. to pregnant mice. Delivery to an assortment of tissues was evaluated using next-generation sequencing. The heatmap depicts mean relative accumulation for each LNP/b-DNA in pregnant mouse tissues, placentas and fetuses ($n = 6$ biological replicates). **c**–**j**, LNP 6 (negative control), LNP 55 (placenta-tropic), LNP 97 (C12-200) and LNP 98 (DLin-MC3-DMA) were formulated with luciferase mRNA and administered to pregnant mice at a dose of 0.6 mg kg^{-1} mRNA; 6 h after administration, tissues, fetuses and placentas were dissected and imaged using IVIS (**c**,**h**). Luminescence was quantified in the lungs (**d**), liver (**e**) and spleen (**f**) and used to calculate a spleen-to-liver ratio (**g**). Luminescence was also quantified in the placentas (**i**) and fetuses (**j**). Representative images are shown from the mouse with luminescence values in the placenta closest to the mean for each treatment group. Luminescence measurements are reported as the mean ± s.e.m. ($n = 4$ biological replicates). Either ordinary (**d**–**g**) or nested (**i**–**j**) two-sided, one-way ANOVAs with post hoc Student's t-tests using the Holm–Šídák correction for multiple comparisons were used to compare luminescence across treatment groups. Dist., distal; F, fetuses; H, heart; K, kidneys; Li, liver; Lum., luminescence; Lu, lungs; P, placentas; Prox., proximal; S, spleen. Illustrations in **a** were created using BioRender (https://biorender.com).

LNPs 6, 55, 97 and 98 were formulated with luciferase mRNA by microfluidic mixing to generate LNPs, the physicochemical properties of which were subsequently characterized (Supplementary Figs. 9 and 10 and Supplementary Table 9). Luciferase mRNA LNPs were administered i.v. to non-pregnant and pregnant mice at an mRNA dose of 0.6 mg kg^{-1}. Six hours following LNP treatment, the heart, lungs, liver, kidneys, spleen, placentas and fetuses were dissected for bioluminescence imaging using an in vivo imaging system (IVIS) (Fig. 1c–j, Extended Data Fig. 3 and Supplementary Figs. 11–13). Consistent with the results from high-throughput screening, LNP 6 mediated minimal luciferase expression across all tissues in non-pregnant and pregnant mice, and LNPs 97 and 98 both facilitated greater luciferase expression in the liver than LNP 55 in non-pregnant mice (Extended Data Fig. 3c). LNP 55 enabled potent luciferase mRNA delivery to the spleen, with significantly greater luminescence than LNPs 97 and 98 in pregnant mice (Fig. 1f). To quantify extrahepatic delivery, we calculated a spleen-to-liver ratio; in both non-pregnant and pregnant mice, the spleen-to-liver ratio for LNP 55 was greater than those for LNPs 6, 97 and 98 (Fig. 1g and Extended Data Fig. 3e). However, the spleen-to-liver ratio was lower in pregnant mice than in non-pregnant mice for LNP 55 (Supplementary Fig. 12d), suggesting that some of this extrahepatic LNP delivery was potentially shifted to other tissues, in particular the placenta.

LNP 55 promoted significantly greater luciferase mRNA delivery to the placenta than the other three LNP treatments tested here, consistent with results from the b-DNA high-throughput screen (Fig. 1i). Specifically, this placenta-tropic LNP mediated more than an order of magnitude greater luciferase mRNA delivery to the placenta compared with the C12-200 industry standard LNP (30-fold improvement) and the DLin-MC3-DMA clinical standard LNP (183-fold improvement). Comparing LNP 55 with previously reported formulations for placental delivery[23,24], we observed that LNP 55 enabled greater luciferase mRNA delivery to the placenta with less luminescence in the liver compared with the previously reported A10 formulation[24] (Supplementary Fig. 14). We did not observe luciferase expression in the fetuses for any of the LNP treatment groups, which is likely to be because of the presence of tight cellular barriers in the placenta[48,49] (Fig. 1h,j and Supplementary Fig. 13).

Mechanism of placental LNP delivery

We next aimed to explore the potential mechanism by which LNP 55 enables mRNA delivery to the placenta. Many LNP formulations achieve liver tropism upon systemic administration because of the formation of an ApoE-rich protein corona[21,50,51]. This is true for the Onpattro LNP therapeutic for hATTR containing the DLin-MC3-DMA ionizable lipid, which promotes ApoE binding and preferential hepatocyte targeting[45,52]. Recent work has indicated that incorporating an anionic phospholipid as a fifth component in the LNP formulation can promote spleen tropism through the formation of a β_2-glycoprotein I (β_2-GPI)-rich protein corona[20,21]. As the placental tropism of LNP 55 was accompanied by splenic delivery, we proposed that the C14-494 ionizable lipid structure in this formulation could promote β_2-GPI binding; in particular, the ether linkages in the structure could impart slight electronegativity to the lipid, serving a similar role to that of an anionic lipid (Supplementary Figs. 1 and 15).

We formulated LNP 55 and the clinical standard DLin-MC3-DMA formulation (LNP 98) with luciferase mRNA and precoated these LNPs with either β_2-GPI or ApoE to evaluate the effects of protein adsorption on luciferase expression and intracellular uptake. In Hep G2 immortalized hepatocytes, LNPs coated with β_2-GPI enabled an approximately 2.7-fold improvement in luciferase expression for LNP 55, but only with higher amounts of protein (Fig. 2a). However, preincubating LNP 98 with ApoEimproved luciferase expression for all amounts of protein tested (Fig. 2b). After assessing mRNA transfection, we labelled LNPs with lipophilic fluorescent dye (DiD) to evaluate intracellular uptake 30 min following treatment; precoating LNP 98 with ApoE enhanced uptake in Hep G2 cells (Fig. 2c and Supplementary Fig. 16a).

We repeated these experiments in immortalized Jurkat T cells, RAW 264.7 macrophages and Raji B cells—to model the main cell types in the spleen—as well as BeWo b30 immortalized trophoblasts, representative of one of the main cell types in the placenta. Preincubating LNPs with β_2-GPI significantly improved LNP-55-mediated luciferase expression in Jurkat, RAW 264.7, Raji and BeWo b30 cells but had no apparent effect for LNP 98 (Fig. 2d and Supplementary Fig. 17a,c,e). Conversely, ApoE preincubation improved luciferase expression for LNP 98 in Jurkat and Raji cells but only at the lowest concentrations of protein tested (Supplementary Fig. 17b,f). Similar but less drastic effects were observed in BeWo b30 and RAW 264.7 cells: ApoE preincubation significantly improved LNP-98-mediated luciferase expression for all amounts of protein tested but had no apparent effect on transfection for LNP 55 (Fig. 2e and Supplementary Fig. 17d). In addition to enhancing mRNA expression, β_2-GPI preincubation promoted greater cellular uptake of DiD-labelled LNP 55 than uncoated LNPs in both Jurkat and BeWo b30 cells (Fig. 2f and Supplementary Fig. 16b–d).

We then sought to explore our proposed mechanism for placental tropism in vivo through β_2-GPI knockdown in pregnant mice. We employed a knockdown rather than a knockout model as β_2-GPI is rapidly synthesized by the placenta during pregnancy and β_2-GPI-knockout mice have been shown to develop fetal growth restriction and compromised placental function[53,54], which could have unintended and confounding consequences for mRNA LNP delivery. Seventy-two hours before LNP administration, pregnant mice were treated i.v. with 1 mg kg^{-1} β_2-GPI siRNA to generate knockdown mice (Supplementary Fig. 18a,b). Pregnant mice were then treated with LNP 55 or 98 at a dose of 0.6 mg kg^{-1} luciferase mRNA, after which tissues, placentas and fetuses were dissected for luminescence imaging by IVIS. For both LNP 55 and LNP 98, β_2-GPI knockdown increased luciferase expression in the liver (Fig. 2g–h), perhaps owing to an increased likelihood of ApoE adsorption. Although β_2-GPI knockdown did not significantly affect LNP-55-mediated mRNA delivery to the placenta (Fig. 3i), knockdown decreased ($P = 0.0407$) luminescence in the placenta for LNP 98 (Fig. 3j). These results could be partially explained by the strong affinity of β_2-GPI for anionic structures and that, as a result of employing a knockdown rather than a knockout model, there was still β_2-GPI present in the circulation at the time of LNP administration that could facilitate LNP tropism.

Cellular LNP delivery in pre-eclampsia

After observing potent in vivo luciferase mRNA delivery to the placenta with LNP 55, we sought to explore the effects of pre-eclampsia on LNP delivery, as maternal blood pressure is elevated in this disease state to compensate for impaired placental vascularization. A low dose of lipopolysaccharide (LPS; 1 μg kg^{-1}) was administered intraperitoneally (i.p.) to pregnant mice on gestational day 7.5 (E7.5) to establish an inflammation-induced model of pre-eclampsia[55–57]. DiD-labelled LNPs encapsulating luciferase mRNA were administered to both healthy and pre-eclamptic mice at an mRNA dose of 1 mg kg^{-1}. Twelve hours following administration, tissues were dissected and imaged using IVIS; DiD fluorescence was used to evaluate LNP biodistribution, whereas luminescence was used to evaluate luciferase mRNA transfection (Fig. 3a–d and Supplementary Figs. 19 and 20). Notably, images of DiD fluorescence showed accumulation of LNP 55 in the liver without evidence of strong luciferase expression (Fig. 4a,b). This suggests that although the first-pass hepatic clearance effect evidently drives LNP accumulation in liver tissue, reduced binding of ApoE to LNP 55 could limit intracellular uptake and subsequent protein expression. Mean DiD fluorescence was greater ($P = 0.0995$) in placentas and significantly greater ($P = 0.0479$) in livers of mice with pre-eclampsia compared with healthy pregnant mice (Supplementary Fig. 20b,d).

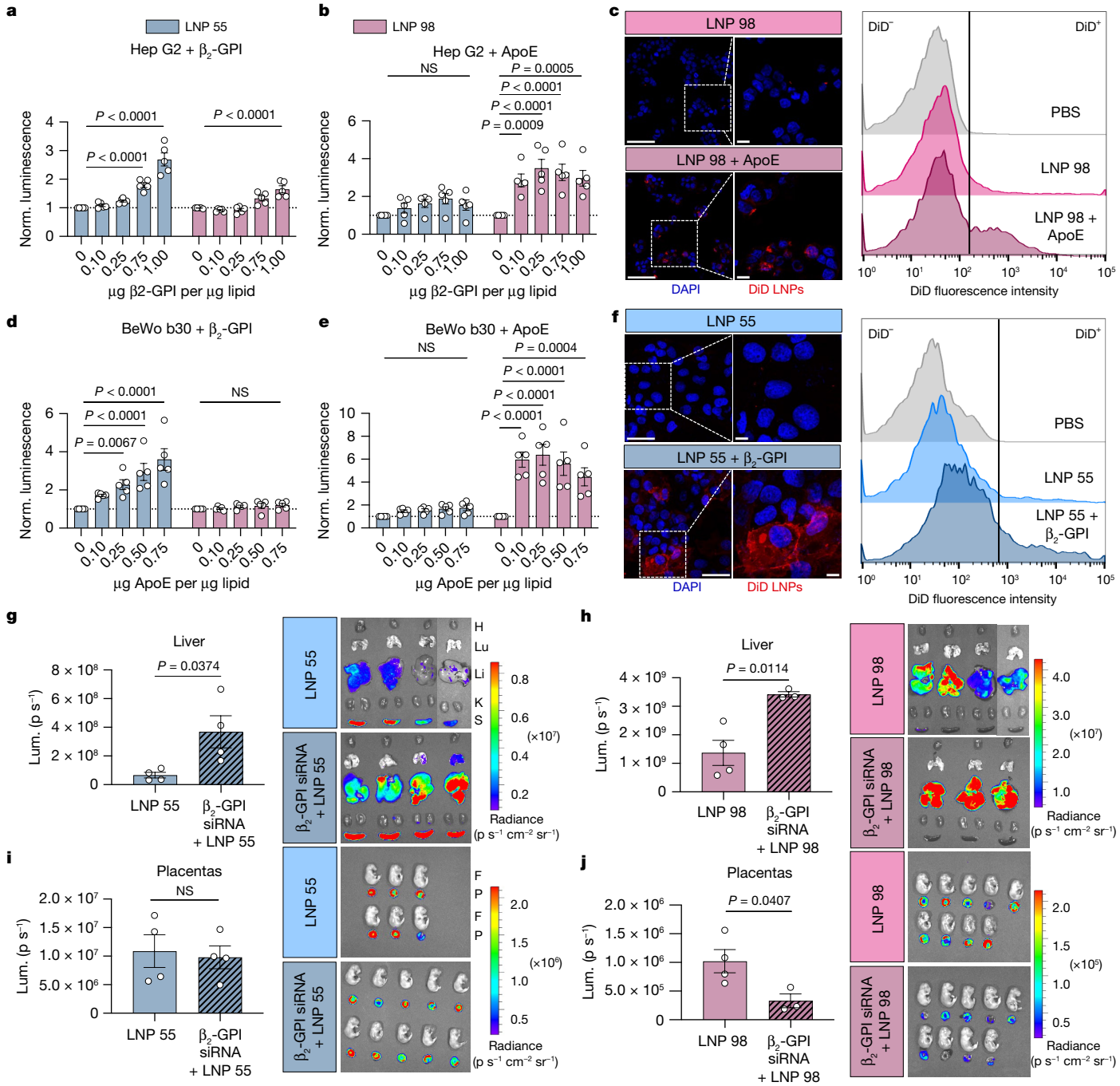

Fig. 2 | A potential protein-adsorption-based endogenous targeting mechanism for LNP delivery to the placenta. a–**f**, LNPs were precoated with either β_2-GPI (**a**,**d**,**f**) or ApoE (**b**,**c**,**e**) and used to treat liver Hep G2 (**a**–**c**) and placenta BeWo b30 cells (**d**–**f**). In **a**, **b**, **d** and **e**, luciferase expression was used to evaluate mRNA expression, whereas in **c** and **f**, confocal microscopy and flow cytometry were used to evaluate intracellular uptake of DiD-labelled LNPs. Normalized luciferase expression is reported as mean ± s.e.m. ($n = 5$ biological replicates with 3–6 technical replicates each). Nested two-sided, one-way ANOVAs with post hoc Student's *t*-tests using the Holm–Šídák correction for multiple comparisons were used to compare normalized luciferase expression across treatment groups. Representative histograms are shown from the technical replicate with the percentage of DiD$^+$ cells closest to the mean for each treatment group. **g**–**j**, To evaluate the effects of in vivo β_2-GPI knockdown on LNP mRNA delivery, 72 h before LNP administration, pregnant mice were treated with 1 mg kg^{-1} β_2-GPI siRNA. Pregnant mice were treated with luciferase mRNA LNPs 55 (**g**,**i**) or 98 (**h**,**j**) at a dose of 0.6 mg kg^{-1} mRNA. Six hours later, tissues were dissected and imaged using IVIS. Luminescence was quantified in the liver (**g**,**h**) and placentas (**i**,**j**). Luminescence is reported as the mean ± s.e.m. (LNP 55, β_2-GPI siRNA + LNP 55, LNP 98: $n = 4$ biological replicates; β_2-GPI siRNA + LNP 98: $n = 3$ biological replicates). Representative images are shown from the mouse with luminescence values in the placenta closest to the mean for each treatment group. Either ordinary (**g**,**h**) or nested (**i**,**j**) unpaired, two-tailed Student's *t*-tests were used to compare luminescence across treatment groups. Lum., luminescence; Norm., normalized. Scale bars, 50 μm (insets, 10 μm).

After assessing organ biodistribution and transfection, we explored LNP delivery to the spleen and placenta—organs in which we observed high luminescence—on a single-cell level using flow cytometry[58] (Supplementary Figs. 21 and 22). Approximately 65% of splenic CD11b$^+$ myeloid cells and CD11b$^+$CD11c$^+$ dendritic cells were DiD$^+$ (Fig. 3e,f), and percentages of DiD$^+$ cells were lower among splenic immune cells ($P = 0.1345$), myeloid cells ($P = 0.1886$), dendritic cells ($P = 0.1312$) and T cells ($P = 0.0419$) in pre-eclampsia compared with healthy mice

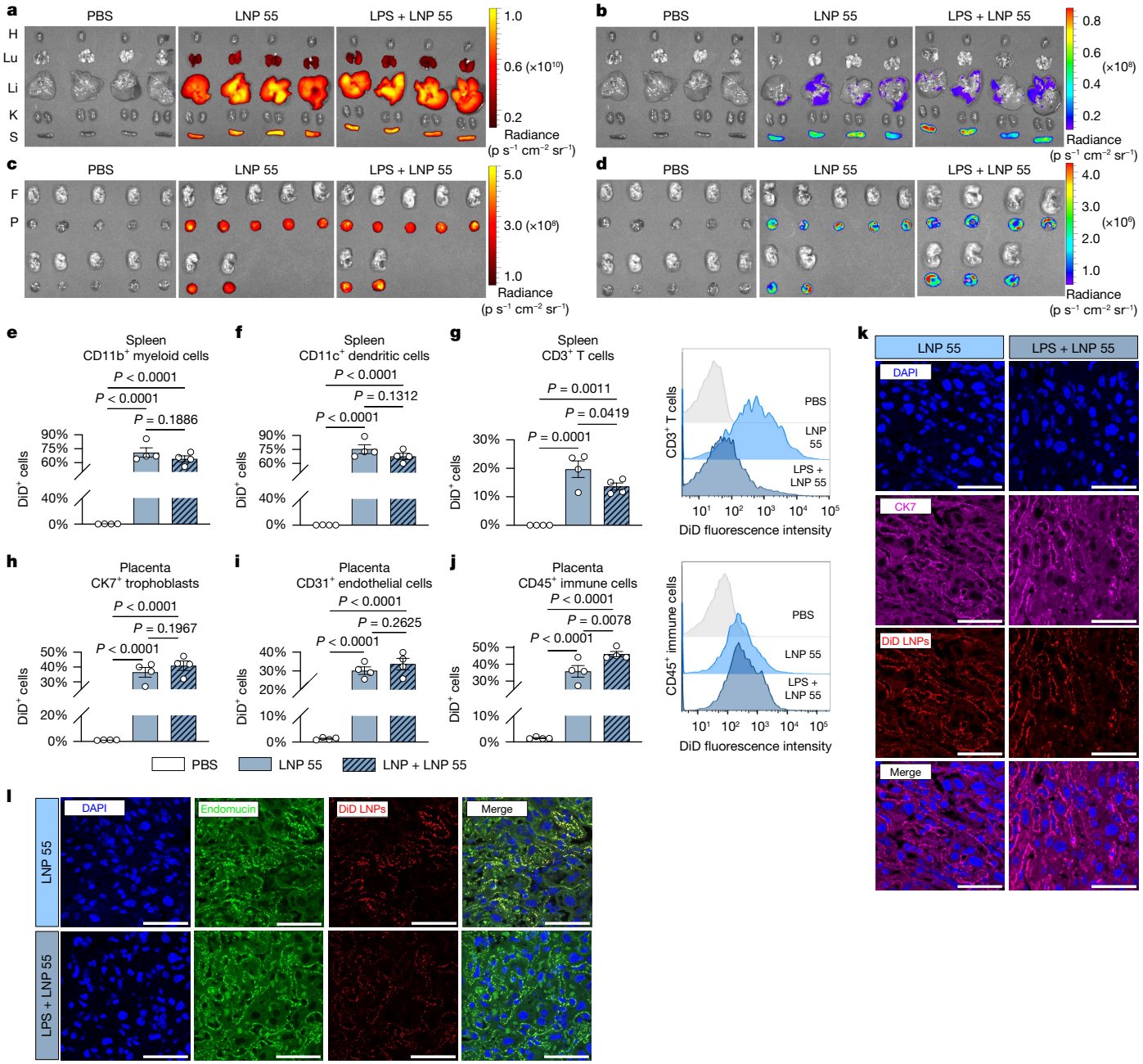

Fig. 3 | Inflammation-induced pre-eclampsia increases LNP 55 delivery to placental immune cells while decreasing off-target delivery to splenic T cells. a–d, To evaluate differences in biodistribution and mRNA transfection between healthy and pre-eclamptic pregnant mice, an early-onset model of pre-eclampsia was induced through i.p. administration of 1 μg kg^{-1} LPS. LNP 55 was formulated with luciferase mRNA, labelled with DiD fluorescent dye and administered at a dose of 1 mg kg^{-1} mRNA. Twelve hours later, tissues (**a**,**b**), placentas and fetuses (**c**,**d**) were dissected, and fluorescence (**a**,**c**) and luminescence (**b**,**d**) imaging was performed. Representative images are shown from the mouse with fluorescence or luminescence values in the placenta (**c**,**d**) closest to the mean for each treatment group. **e–l**, Cellular LNP delivery was evaluated in splenic myeloid cells (**e**), dendritic cells (**f**), and T cells (**g**) as well as placental trophoblasts (**h**), endothelial cells (**i**), and immune cells (**j**) by flow cytometry. The percentage of DiD$^+$ cells is reported as the mean ± s.e.m. ($n = 4$ biological replicates). Representative histograms for splenic CD3$^+$ T cells (**g**) and placental CD45$^+$ immune cells (**j**) are shown from samples with the percentage of DiD$^+$ cells closest to the mean for each treatment group. Immunofluorescence staining of placental sections for pan-trophoblast marker cytokeratin 7 (CK7) (**k**) and an endothelial cell marker (endomucin) (**l**) demonstrated colocalization of placental cells and DiD-labelled LNPs. Either ordinary (**e–g**) or nested (**h–j**) two-sided, one-way ANOVAs with post hoc Student's *t*-tests using the Holm–Šídák correction for multiple comparisons were used to compare the percentages of DiD$^+$ cells across treatment groups. Scale bars, 50 μm.

(Fig. 3e–g and Supplementary Fig. 23a). These results are encouraging, suggesting the potential for less off-target LNP 55 delivery to splenic T cells in pre-eclampsia.

In the placenta, trophoblasts, endothelial cells and immune cells are all responsible for regulating angiogenesis and vascularization, making them important cellular targets for VEGF mRNA LNP therapy[59]. In contrast to the results observed in the spleen, pre-eclampsia seemed to improve LNP 55 delivery to placental cells. There were no significant differences in the percentages of DiD$^+$ cells in placental trophoblasts ($P = 0.1967$) and endothelial cells ($P = 0.2625$), yet we observed significantly greater DiD positivity in placental immune cells ($P = 0.0078$) in pre-eclamptic mice than in healthy mice (Fig. 3h–j). This could perhaps

be explained by the trafficking of phagocytic immune cells such as macrophages to the placenta in pre-eclampsia[60]. In addition, pregnant mice with inflammation-induced pre-eclampsia had higher ($P = 0.0015$) serum levels of β_2-GPI (Supplementary Fig. 18c), which could partially explain the increase in LNP 55 delivery to placental immune cells in pre-eclampsia. Immunofluorescence staining of placental tissue sections was also used to visualize delivery of DiD-labelled LNP 55 to the placental vasculature. Consistent with flow cytometry results, we observed colocalization of DiD LNPs with regions stained positive for cytokeratin 7 (CK7, trophoblasts) and endomucin (endothelial cells) (Fig. 3k–l).

Finally, we repeated these assays to evaluate cellular delivery in the spleen and placenta with the standard LNP formulations 97 and 98 (Extended Data Fig. 4). Relative to LNP 55, LNP 97 mediated comparable DiD positivity in splenic myeloid, dendritic and T cells, with a lower proportion of DiD^+ cells in the placenta (Extended Data Fig. 4a–c,g–i). Notably, LNP 97 facilitated delivery to approximately 25% of trophoblasts in the placenta but only about 5% of endothelial cells (Extended Data Fig. 4g–h). Conversely, only about 30–40% of splenic myeloid and dendritic cells were DiD^+ following treatment with LNP 98, and no DiD positivity was detectable in the placenta (Extended Data Fig. 4d–f,j–l).

VEGF mRNA LNP therapy for pre-eclampsia

We next explored the application of LNP 55 as a therapeutic for treating pre-eclampsia by means of VEGF mRNA delivery to the placenta. First, as it is critical to identify the minimum effective dose rather than the maximum tolerated dose for pregnant patients, we evaluated the safety and potency of three therapeutic doses—0.2, 1.0 and 2.0 mg kg^{-1} VEGF mRNA—in healthy pregnant mice (Supplementary Fig. 24). Six hours after i.v. administration, the 1.0 mg kg^{-1} and 2.0 mg kg^{-1} treatments increased serum VEGF levels by more than ten-fold and more than 50-fold, respectively, compared with those of untreated mice. As there was minimal evidence of dose-dependent inflammation, liver injury or vascular permeability in the placenta, we opted to further pursue the 1.0 mg kg^{-1} VEGF mRNA therapeutic in both inflammation- and hypoxia-induced models of pre-eclampsia.

Inflammation-induced pre-eclampsia was established by i.p. administration of 1 μg kg^{-1} LPS[55–57] (Fig. 4a). Starting on gestational day E13, pre-eclamptic mice treated with VEGF mRNA LNP 55 had significantly greater daily change in weight than the LPS-only treatment group (Extended Data Fig. 5a and Supplementary Table 10). Blood pressure is used as a primary outcome for animal models of pre-eclampsia, as hypertension during pregnancy is a key clinical indicator of the disease[1]. After LPS administration on E7.5, blood pressure increased significantly compared with that of healthy mice and remained elevated until the end of gestation (Fig. 4b and Supplementary Table 11). A single injection of VEGF mRNA LNP 55 immediately and permanently alleviated maternal hypertension in pre-eclamptic mice until the end of gestation. Mice were euthanized before parturition on E17 to evaluate fetal and placental weight (Fig. 4c–e and Extended Data Fig. 5b,c). Litter size was lower for pre-eclamptic mice than in healthy pregnancy; this reduction in litter size was partially dispelled by treatment with VEGF mRNA LNP 55. VEGF mRNA LNP 55 also significantly increased total litter weight compared with that of pre-eclamptic mice.

On gestational day E11.5, six hours following administration of VEGF mRNA LNP 55, serum VEGF levels were elevated compared with those of the phosphate-buffered saline (PBS) and LPS treatment groups, indicating successful expression of VEGF and secretion into circulation (Extended Data Fig. 5d). We also assessed serum levels of sFlt-1 and the liver enzymes alanine transaminase (ALT) and aspartate aminotransferase (AST) but observed no significant differences among treatment groups (Extended Data Fig. 5e–g). Similarly, we measured serum cytokine levels to evaluate LNP-mediated inflammation. On gestational day E11.5, serum levels of tumour necrosis factor (TNF), interleukin-6 (IL-6) and interferon-γ (IFNγ) were all significantly elevated in pre-eclampsia compared with healthy pregnancies, whereas administration of the VEGF mRNA LNP 55 therapeutic was able to reverse this effect for the IL-6 and IFNγ cytokines (Extended Data Fig. 5h–j). Finally, haematoxylin and eosin (H&E) staining of placental sections was used to visualize vasculature in the placental labyrinth; VEGF mRNA LNP 55 demonstrated improvements in mean blood vessel area in the placenta compared with pre-eclamptic mice (Fig. 4f and Extended Data Fig. 5k).

Hypoxia-induced pre-eclampsia was established through overexpression of sFlt-1 as a result of i.v. administration of 1×10^9 plaque-forming units (PFU) of sFlt-1 adenovirus (Adv-sFlt-1)[6,61] (Fig. 4a). Throughout gestation, there were no significant differences in daily maternal weight change among treatment groups, but as with the inflammation-induced model, mean blood pressure increased immediately after inducing pre-eclampsia (Fig. 4g and Extended Data Fig. 6a). Following the administration of VEGF mRNA LNPs, mean blood pressure decreased for mice treated with LNP 55 and LNP 98; however, VEGF mRNA LNP 55 was able to eliminate hypertension until the end of gestation, whereas the blood pressure of mice treated with VEGF mRNA LNP 98 mice gradually approached that of the Adv-sFlt-1 cohort towards the end of gestation (Fig. 4g and Supplementary Table 13). Although no significant differences in total litter weight or litter size were observed across treatment groups (Extended Data Fig. 6b,c), fetal and placental weight distributions indicated that fetal weight was generally lower and placental weight was generally higher for Adv-sFlt-1-treated mice; both of these effects were diminished by VEGF mRNA LNP 55 treatment (Fig. 4h–j).

Consistent with our data demonstrating that LNP 98 is a potent liver-tropic formulation, VEGF mRNA LNP 98 facilitated a more than four-fold greater concentration of VEGF in serum compared with the placenta-tropic LNP 55 on gestational day E11.5 (Extended Data Fig. 6e). By the model endpoint on gestational day E17, serum sFlt-1 levels were elevated more than ten-fold for pre-eclamptic mice compared with healthy pregnancies (Fig. 4k). VEGF mRNA LNP 55 reduced sFlt-1 levels in serum, whereas there were no significant differences between pre-eclamptic mice and those treated with VEGF mRNA LNP 98. This hypoxia-induced model of pre-eclampsia may also partially recapitulate HELLP syndrome, as liver enzymes ALT and AST were both elevated on gestational day E17 compared with healthy pregnant mice (Extended Data Fig. 6f,g). VEGF mRNA LNPs 55 and 98 both decreased the concentrations of these enzymes during pre-eclampsia, but serum AST levels remained elevated compared to healthy pregnancy in mice treated with VEGF mRNA LNP 98. Other than a slight increase in serum IL-6 concentration 6 h following LNP 55 administration, there were no significant differences in the serum concentration of inflammatory cytokines across treatment groups (Extended Data Fig. 6h–j). As in the LPS-induced model of pre-eclampsia, H&E staining of placental sections and quantification of mean blood vessel area showed that VEGF mRNA LNP 55 increased placental blood vessel area compared with that of Adv-sFlt-1-treated pre-eclamptic mice (Extended Data Fig. 6k).

In this hypoxia-induced model, we also assessed renal damage through histology and proteinuria, as an elevated concentration of protein in urine is often used as a further diagnostic criterion for pre-eclampsia in the clinic. The concentration of albumin in urine was elevated in Adv-sFlt-1 pre-eclamptic mice compared with healthy pregnant mice, and H&E staining of kidney tissue suggested some potential kidney injury (Extended Data Fig. 6d,l). For example, kidneys from Adv-sFlt-1-treated mice showed signs of enlarged glomeruli and swollen glomerular endothelial cells, effects that seemed to be partially alleviated by treatment with VEGF mRNA LNPs.

Pre-eclampsia immune landscape modulation

As we observed evidence of red blood cell accumulation and immune infiltration in the placenta in the inflammation-induced model of

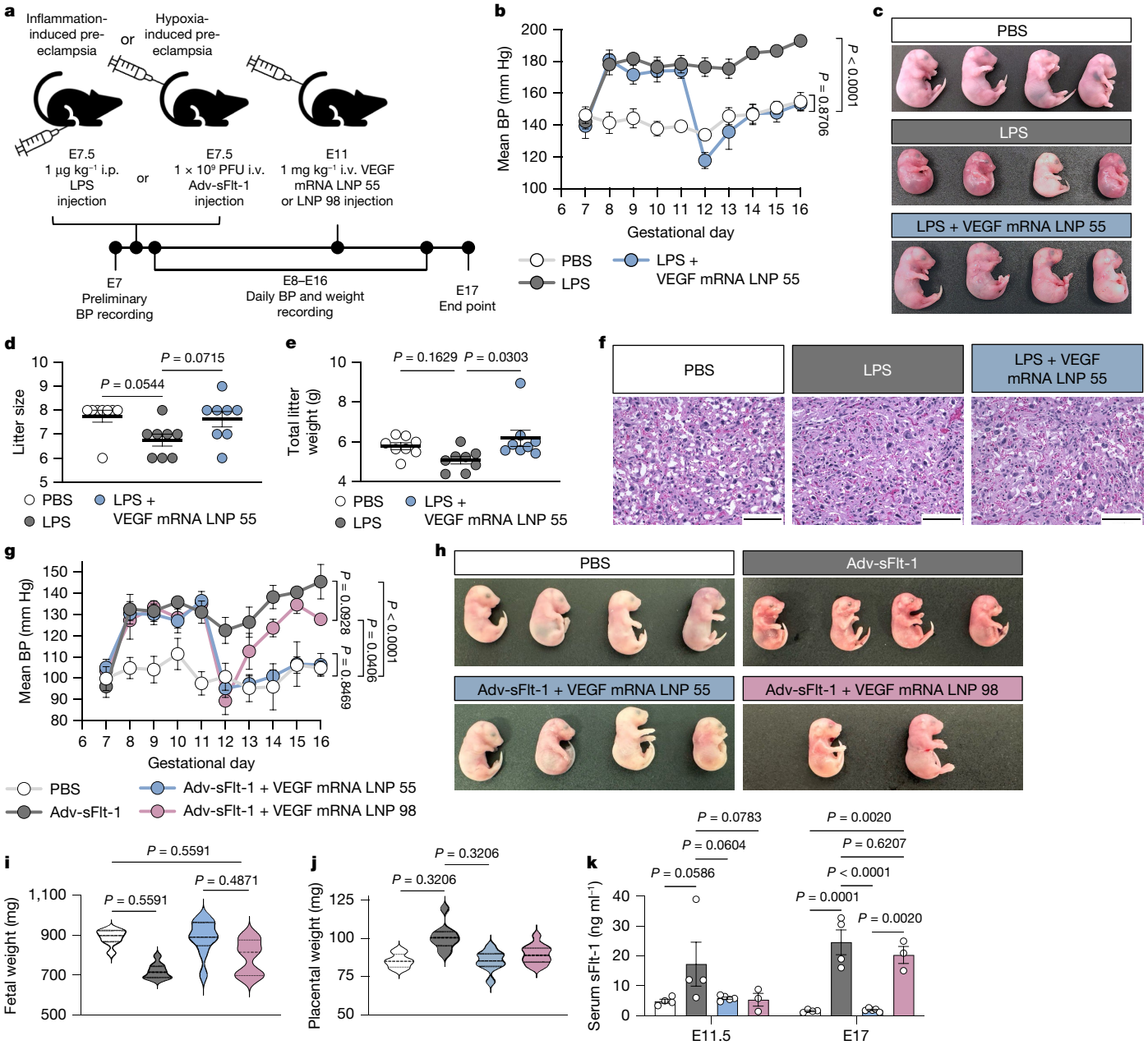

Fig. 4 | VEGF mRNA LNP 55 alleviates maternal hypertension in inflammation- and hypoxia-induced models of pre-eclampsia. a, Inflammation-induced pre-eclampsia was established through i.p. administration of 1 μg kg^{-1} LPS, whereas hypoxia-induced pre-eclampsia was established through i.v. administration of 1×10^9 PFU of Adv-sFlt-1 on gestational day E7.5. Then, VEGF mRNA LNP 55 or LNP 98 was administered i.v. on gestational day E11 at an mRNA dose of 1 mg kg^{-1}. **b**,**g**, In both inflammation-induced (**b**) and hypoxia-induced (**g**) pre-eclampsia, maternal blood pressure (BP) was recorded daily, and on gestational day E17, litter size (**d**), total litter weight (**e**), fetal weight (**i**) and placental weight (**j**) were recorded. In **c** and **h**, representative fetus images are shown from the mouse with the total litter weight or fetal weight measurements closest to the mean for each treatment group. **f**, Placental vasculature in the labyrinth was visualized with H&E staining. **k**, Serum levels of sFlt-1 were evaluated on gestational days E11.5 and E17. For the inflammation-induced model of pre-eclampsia, mean BP, litter size and total litter weight are reported as mean ± s.e.m. ($n = 8$ biological replicates). For the hypoxia-induced model of pre-eclampsia, mean BP and serum levels of sFlt-1 are reported as mean ± s.e.m. (Adv-sFlt-1 + VEGF mRNA LNP 55: $n = 5$ biological replicates; PBS, Adv-sFlt-1: $n = 4$ biological replicates; Adv-sFlt-1 + VEGF mRNA LNP 98: $n = 3$ biological replicates). Fetal and placental weights are reported as medians with 25th and 75th percentiles (2–12 fetuses or placentas per mouse). Ordinary (**d**,**e**) or nested (**i**,**j**) two-sided, one-way ANOVAs or ordinary two-sided, two-way ANOVAs (**b**,**g**,**k**) with post hoc Student's *t*-tests using the Holm–Šídák correction for multiple comparisons were used to compare responses across treatment groups. Scale bars, 100 μm. The illustration of mice and syringes in **a** was created using Microsoft PowerPoint stock icons.

pre-eclampsia (Fig. 4f), we sought to characterize the immune landscape in the blood, spleen and placenta in these models (Extended Data Fig. 7 and Supplementary Figs. 25–28). First, in the LPS model, we evaluated immune cell populations in the blood, including the percentages of CD19$^+$ B cells, CD3$^+$ T cells, CD11b$^+$ myeloid cells and CD11b$^+$CD11c$^+$ dendritic cells, all of which were significantly elevated in pre-eclampsia compared with healthy mice (Extended Data Fig. 7a). VEGF mRNA LNP 55 reduced the percentages of both T cells and dendritic cells in the blood, shifting the immune landscape closer to that of healthy mice. In the spleen, the percentage of CD11b$^+$ myeloid cells was significantly elevated for LPS-treated mice, as well as for the VEGF mRNA LNP treatment group compared with healthy pregnant mice

(Extended Data Fig. 7b). This expansion of myeloid cells in the spleen was probably a result of LPS-induced systemic and local inflammation in this model of pre-eclampsia, consistent with previous reports of myeloid cell expansion in the spleen as a result of inflammatory conditions[62]. In the placenta, the percentages of $CD19^+$ B cells, $CD3^+$ T cells and $CD11c^+$ dendritic cells were all significantly elevated in pre-eclampsia (Extended Data Fig. 7c). Administration of VEGF mRNA LNPs then reduced the proportion of B cells and T cells in the placenta to those observed in healthy mice.

As the hypoxia-induced model of pre-eclampsia we employed is far less immune-implicated than the inflammation-induced model, we observed few significant changes in immune cell population frequencies in the blood and spleen (Supplementary Figs. 27a,b and 28). However, in the placentas, fractions of $CD19^+$ B cells, $CD3^+$ T cells, $CD11b^+$ myeloid cells and $CD11c^+$ dendritic cells were all elevated in the Adv-sFlt-1 and VEGF mRNA LNP 55 treatment groups (Supplementary Fig. 27c). These results indicate possible immune cell infiltration to the placenta in pre-eclampsia; in the future, this could be more thoroughly explored and perhaps addressed using a second-generation placenta-tropic therapeutic.

Conclusions

LNPs are the most clinically advanced non-viral platform for mRNA delivery and have been used in a variety of clinical applications including infectious disease vaccines, protein replacement therapies and gene editing therapeutics[63,64]. However, LNPs have been minimally explored with respect to women's health applications, particularly for conditions occurring during pregnancy. Here we aimed to develop a VEGF mRNA LNP therapeutic to remodel placental vasculature to treat pre-eclampsia during pregnancy. To this end, we used high-throughput in vivo screening to identify LNP 55, a placenta-tropic LNP formulation that enabled a 183-fold improvement in mRNA delivery to the placenta compared with the clinically approved DLin-MC3-DMA LNP formulation. We propose a potential protein-adsorption-based endogenous targeting mechanism that may facilitate mRNA delivery to the placenta. In an inflammation-induced mouse model of pre-eclampsia, off-target LNP delivery to the spleen was reduced while on-target delivery to placental immune cells was improved compared to healthy pregnant mice. Finally, through delivery of VEGF mRNA, this LNP platform rescued maternal hypertension in multiple mouse models of pre-eclampsia with a single i.v. injection.

Approximately 800 women die from pregnancy- or childbirth-related conditions every day, with the vast majority of these deaths occurring in developing countries owing to hypertensive pregnancy disorders such as pre-eclampsia and eclampsia[65]. Although future work will focus on translating this mRNA LNP technology, preliminary results evaluating the shelf-life of LNP 55 are encouraging and suggest that potent mRNA delivery is retained over a 6 week period and after multiple freeze–thaw cycles (Supplementary Fig. 29). Here we engineered an easy-to-manufacture LNP platform that enables potent mRNA delivery to the placenta upon simple i.v. administration, a potentially broadly translatable therapeutic with key advantages over previous approaches that have required more invasive injection into the intrauterine artery for viral-vector-mediated gene therapy[9–11]. This work demonstrates the potential application of a placenta-tropic mRNA LNP platform for the treatment of obstetric disorders such as pre-eclampsia.

Online content

Any methods, additional references, Nature Portfolio reporting summaries, source data, extended data, supplementary information, acknowledgements, peer review information; details of author contributions and competing interests; and statements of data and code availability are available at https://doi.org/10.1038/s41586-024-08291-2.

1. Chappell, L. C., Cluver, C. A., Kingdom, J. & Tong, S. Pre-eclampsia. *Lancet* **398**, 341–354 (2021).
2. Swingle, K. L., Ricciardi, A. S., Peranteau, W. H. & Mitchell, M. J. Delivery technologies for women's health applications. *Nat. Rev. Bioeng.* **1**, 408–425 (2023).
3. Adams, D. et al. Patisiran, an RNAi therapeutic, for hereditary transthyretin amyloidosis. *New Engl. J. Med.* **379**, 11–21 (2018).
4. Geisler, H. C., Safford, H. C. & Mitchell, M. J. Rational design of nanomedicine for placental disorders: birthing a new era in women's reproductive health. *Small* **20**, 2300852 (2023).
5. Gilbert, J. S. et al. Recombinant vascular endothelial growth factor 121 infusion lowers blood pressure and improves renal function in rats with placentalischemia-induced hypertension. *Hypertension* **55**, 380–385 (2010).
6. Mateus, J. et al. Endothelial growth factor therapy improves preeclampsia-like manifestations in a murine model induced by overexpression of sVEGFR-1. *Am. J. Physiol. Heart Circ. Physiol.* **301**, H1781–H1787 (2011).
7. Li, Z. et al. Recombinant vascular endothelial growth factor 121 attenuates hypertension and improves kidney damage in a rat model of preeclampsia. *Hypertension* **50**, 686–692 (2007).
8. David, A. L. et al. Local delivery of VEGF adenovirus to the uterine artery increases vasorelaxation and uterine blood flow in the pregnant sheep. *Gene Ther.* **15**, 1344–1350 (2008).
9. David, A. L. Maternal uterine artery VEGF gene therapy for treatment of intrauterine growth restriction. *Placenta* **59**, S44–S50 (2017).
10. Mehta, V. et al. Long-term increase in uterine blood flow is achieved by local overexpression of VEGF-A 165 in the uterine arteries of pregnant sheep. *Gene Ther.* **19**, 925–935 (2012).
11. Carr, D. J. et al. Uteroplacental adenovirus vascular endothelial growth factor gene therapy increases fetal growth velocity in growth-restricted sheep pregnancies. *Hum. Gene Ther.* **25**, 375–384 (2014).
12. Woods, A. K. et al. Adenoviral delivery of VEGF121 early in pregnancy prevents spontaneous development of preeclampsia in BPH/5 mice. *Hypertension* **57**, 94–102 (2011).
13. Haase, N. et al. RNA interference therapeutics targeting angiotensinogen ameliorate preeclamptic phenotype in rodent models. *J. Clin. Invest.* **130**, 2928–2942 (2020).
14. Turanov, A. A. et al. RNAi modulation of placental sFLT1 for the treatment of preeclampsia. *Nat. Biotechnol.* **36**, 1164–1173 (2018).
15. Yin, H. et al. Non-viral vectors for gene-based therapy. *Nat. Rev. Genet.* **15**, 541–555 (2014).
16. Swingle, K. L., Hamilton, A. G. & Mitchell, M. J. Lipid nanoparticle-mediated delivery of mRNA therapeutics and vaccines. *Trends Mol. Med.* **27**, 616–617 (2021).
17. Polack Fernando, P. et al. Safety and efficacy of the BNT162b2 mRNA Covid-19 vaccine. *New Engl. J. Med.* **383**, 2603–2615 (2020).
18. Baden Lindsey, R. et al. Efficacy and safety of the mRNA-1273 SARS-CoV-2 vaccine. *New Engl. J. Med.* **384**, 403–416 (2021).
19. Sato, Y., Kinami, Y., Hashiba, K. & Harashima, H. Different kinetics for the hepatic uptake of lipid nanoparticles between the apolipoprotein E/low density lipoprotein receptor and the *N*-acetyl-D-galactosamine/asialoglycoprotein receptor pathway. *J. Control. Release* **322**, 217–226 (2020).
20. Cheng, Q. et al. Selective organ targeting (SORT) nanoparticles for tissue-specific mRNA delivery and CRISPR–Cas gene editing. *Nat. Nanotechnol.* **15**, 313–320 (2020).
21. Dilliard, S. A., Cheng, Q. & Siegwart, D. J. On the mechanism of tissue-specific mRNA delivery by selective organ targeting nanoparticles. *Proc. Natl Acad. Sci. USA* **118**, e2109256118 (2021).
22. LoPresti, S. T., Arral, M. L., Chaudhary, N. & Whitehead, K. A. The replacement of helper lipids with charged alternatives in lipid nanoparticles facilitates targeted mRNA delivery to the spleen and lungs. *J. Control. Release* **345**, 819–831 (2022).
23. Swingle, K. L. et al. Ionizable lipid nanoparticles for in vivo mRNA delivery to the placenta during pregnancy. *J. Am. Chem. Soc.* https://doi.org/10.1021/jacs.2c12893 (2023).
24. Young, R. E. et al. Systematic development of ionizable lipid nanoparticles for placental mRNA delivery using a design of experiments approach. *Bioact. Mater.* **34**, 125–137 (2024).
25. Chaudhary, N. et al. Lipid nanoparticle structure and delivery route during pregnancy dictate mRNA potency, immunogenicity, and maternal and fetal outcomes. *Proc. Natl Acad. Sci. USA* **121**, e2307810121 (2024).
26. Safford, H. C. et al. Orthogonal design of experiments for engineering of lipid nanoparticles for mRNA delivery to the placenta. *Small* **20**, e2303568 (2024).
27. Geisler, H. C. et al. EGFR-targeted ionizable lipid nanoparticles enhance in vivo mRNA delivery to the placenta. *J. Control. Release* **371**, 455–469 (2024).
28. Paunovska, K. et al. A direct comparison of in vitro and in vivo nucleic acid selivery mediated by hundreds of nanoparticles reveals a weak correlation. *Nano Lett.* **18**, 2148–2157 (2018).
29. Dahlman, J. E. et al. Barcoded nanoparticles for high throughput in vivo discovery of targeted therapeutics. *Proc. Natl Acad. Sci. USA* **114**, 2060–2065 (2017).
30. Huayamares, S. G. et al. High-throughput screens identify a lipid nanoparticle that preferentially delivers mRNA to human tumors in vivo. *J. Control. Release* **357**, 394–403 (2023).
31. El-Mayta, R. et al. A nanoparticle platform for accelerated in vivo oral delivery screening of nucleic acids. *Adv. Ther.* **4**, 2000111 (2021).
32. Love, K. T. et al. Lipid-like materials for low-dose, in vivo gene silencing. *Proc. Natl Acad. Sci. USA* **107**, 1864–1869 (2010).
33. Semple, S. C. et al. Rational design of cationic lipids for siRNA delivery. *Nat. Biotechnol.* **28**, 172–176 (2010).
34. Jayaraman, M. et al. Maximizing the potency of siRNA lipid nanoparticles for hepatic gene silencing in vivo. *Angew. Chem.* **124**, 8657–8661 (2012).
35. Dusse, L. M. et al. Revisiting HELLP syndrome. *Clin. Chim. Acta* **451**, 117–120 (2015).
36. Fenton, O. S. et al. Synthesis and biological evaluation of ionizable lipid materials for the in vivo delivery of messenger RNA to B lymphocytes. *Adv. Mater.* **29**, 1606944 (2017).

37. Xue, L. et al. Rational design of bisphosphonate lipid-like materials for mRNA delivery to the bone microenvironment. *J. Am. Chem. Soc.* **144**, 9926–9937 (2022).
38. Kauffman, K. J. et al. Optimization of lipid nanoparticle formulations for mRNA delivery in vivo with fractional factorial and definitive Sscreening designs. *Nano Lett.* **15**, 7300–7306 (2015).
39. Billingsley, M. M. et al. Orthogonal design of experiments for optimization of lipid nanoparticles for mRNA engineering of CAR T cells. *Nano Lett.* **22**, 533–542 (2022).
40. Swingle, K. L. et al. Amniotic fluid stabilized lipid nanoparticles for in utero intra-amniotic mRNA delivery. *J. Control. Release* **341**, 616–633 (2022).
41. Veiga, N. et al. Cell specific delivery of modified mRNA expressing therapeutic proteins to leukocytes. *Nat. Commun.* **9**, 4493 (2018).
42. Parhiz, H. et al. PECAM-1 directed re-targeting of exogenous mRNA providing two orders of magnitude enhancement of vascular delivery and expression in lungs independent of apolipoprotein E-mediated uptake. *J. Control. Release* **291**, 106–115 (2018).
43. Shi, D., Toyonaga, S. & Anderson, D. G. In vivo RNA delivery to hematopoietic stem and progenitor cells via targeted lipid nanoparticles. *Nano Lett.* **23**, 2938–2944 (2023).
44. Breda, L. et al. In vivo hematopoietic stem cell modification by mRNA delivery. *Science* **381**, 436–443 (2023).
45. Cullis, P. R. & Hope, M. J. Lipid nanoparticle systems for enabling gene therapies. *Mol. Ther.* **25**, 1467–1475 (2017).
46. Irvin-Choy, N. S., Nelson, K. M., Dang, M. N., Gleghorn, J. P. & Day, E. S. Gold nanoparticle biodistribution in pregnant mice following intravenous administration varies with gestational age. *Nanomed. Nanotechnol. Biol. Med.* **36**, 102412 (2021).
47. Raz, T. et al. The hemodynamic basis for positional- and inter-fetal dependent effects in dual arterial supply of mouse pregnancies. *PLoS ONE* **7**, e52273 (2012).
48. Kertschanska, S., Kosanke, G. & Kaufmann, P. Pressure dependence of so-called transtrophoblastic channels during fetal perfusion of human placental villi. *Microsc. Res. Tech.* **38**, 52–62 (1997).
49. Kertschanska, S., Stulcová, B., Kaufmann, P. & Stulc, J. Distensible transtrophoblastic channels in the rat placenta. *Placenta* **21**, 670–677 (2000).
50. Francia, V., Schiffelers, R. M., Cullis, P. R. & Witzigmann, D. The biomolecular corona of lipid nanoparticles for gene therapy. *Bioconjug. Chem.* **31**, 2046–2059 (2020).
51. Bashiri, G. et al. Nanoparticle protein corona: from structure and function to therapeutic targeting. *Lab Chip* **23**, 1432–1466 (2023).
52. Akinc, A. et al. Targeted delivery of RNAi therapeutics with endogenous and exogenous ligand-based mechanisms. *Mol. Ther.* **18**, 1357–1364 (2010).
53. Chamley, L. W., Allen, J. L. & Johnson, P. M. Synthesis of β_2 glycoprotein 1 by the human placenta. *Placenta* **18**, 403–410 (1997).
54. Robertson, S. A. et al. Effect of β_2-glycoprotein I null mutation on reproductive outcome and antiphospholipid antibody-mediated pregnancy pathology in mice. *Mol. Hum. Reprod.* **10**, 409–416 (2004).
55. Waker, C. A., Kaufman, M. R. & Brown, T. L. Current state of preeclampsia mouse models: approaches, relevance, and standardization. *Front. Physiol.* **12**, 681632 (2021).
56. Ding, X., Yang, Z., Han, Y. & Yu, H. Correlation of long-chain fatty acid oxidation with oxidative stress and inflammation in pre-eclampsia-like mouse models. *Placenta* **36**, 1442–1449 (2015).
57. Huai, J., Yang, Z., Yi, Y.-H. & Wang, G.-J. Different effects of pravastatin on preeclampsia-like symptoms in different mouse models. *Chin. Med. J. (Engl.)* **131**, 461–470 (2018).
58. Swingle, K. L., Hamilton, A. G. & Mitchell, M. J. Flow cytometric analysis of the murine placenta to evaluate nanoparticle platforms during pregnancy. *Placenta* https://doi.org/10.1016/j.placenta.2024.08.007 (2024).
59. Umapathy, A., Chamley, L. W. & James, J. L. Reconciling the distinct roles of angiogenic/anti-angiogenic factors in the placenta and maternal circulation of normal and pathological pregnancies. *Angiogenesis* **23**, 105–117 (2020).
60. Aneman, I. et al. Mechanisms of key innate immune cells in early- and late-onset preeclampsia. *Front. Immunol.* **11**, 1864 (2020).
61. Bergmann, A. et al. Reduction of circulating soluble Flt-1 alleviates preeclampsia-like symptoms in a mouse model. *J. Cell. Mol. Med.* **14**, 1857–1867 (2010).
62. Wu, H. et al. Arginase-1-dependent promotion of TH17 differentiation and disease progression by MDSCs in systemic lupus erythematosus. *Sci. Transl. Med.* **8**, 331ra40 (2016).
63. Hamilton, A. G., Swingle, K. L. & Mitchell, M. J. Biotechnology: overcoming biological barriers to nucleic acid delivery using lipid nanoparticles. *PLoS Biol.* **21**, e3002105 (2023).
64. Yan, Y. et al. Non-viral vectors for RNA delivery. *J. Control. Release* **342**, 241–279 (2022).
65. Stefanovic, V. International Academy of Perinatal Medicine (IAPM) guidelines for screening, prediction, prevention and management of pre-eclampsia to reduce maternal mortality in developing countries. *J. Perinat. Med.* **51**, 164–169 (2023).

Methods

Ionizable lipid synthesis

DLin-MC3-DMA was purchased from Cayman Chemical. All other ionizable lipids were synthesized as previously described[32]. Briefly, the polyamine core (1 equiv., Enamine) was combined with excess alkyl epoxide (7 equiv., MilliporeSigma) in ethanol in 4 ml glass scintillation vials under gentle sitting with a magnetic stir bar for 2 days at 80 °C. The polyamine cores used in this work were 3-[4-(3-{[2-(4-{3-[4-(3-aminopropyl)piperazin-1-yl]propyl}piperazin-1 yl)ethyl]amino}propyl)piperazin-1-yl]propan-1-amine (denoted by 480), 1-N-{2-[4-(4-aminocyclohexyl)piperazin-1-yl]ethyl} cyclohexane-1,4-diamine (denoted by 482), {2-[2-(2-aminoethoxy) ethoxy]ethyl}[2-(4-{2-[2-(2-aminoethoxy)ethoxy]ethyl}piperazin-1-yl) ethyl]amine (denoted by 488), 10-(4-{2-[(10-aminodecyl)amino]ethyl} piperazin-1-yl)decan-1-amine (denoted by 489), 3-(4-{2-[(3-amino-2-ethoxypropyl)amino]ethyl}piperazin-1-yl)-2-ethoxypropan-1-amine (denoted by 490), [1-({[2-(4-{[1-(aminomethyl)cyclohexyl]methyl} piperazin-1-yl)ethyl]amino}methyl)cyclohexyl]methanamine (denoted by 493), 2-{2-[4-(2-{[2-(2-aminoethoxy)ethyl]amino}ethyl)piperazin-1-yl]ethoxy}ethan-1-amine (denoted by 494) and 1-[4-(3-{2-[2-(3-aminopropoxy)ethoxy]ethoxy}propyl)piperazin-1-yl]-7,10,13-trioxa-3-azahexadecan-16-amine (denoted by 497) (Supplementary Fig. 1). The alkyl epoxide tails used in this work were 1,2-epoxydodecane (denoted by C12), 1,2-epoxytetradecane (denoted by C14) and 1,2-epoxyhexadecane (denoted by C16). After 2 days, solvent was evaporated using a Rotovapor R-300 rotary evaporator (Buchi) to isolate crude product. Liquid chromatography mass spectrometry spectra (Supplementary Fig. 2) were acquired to confirm molecular identity using an SQD equipped with an Acquity UPLC using a C8 column, with a 2 min wash followed by a gradient mobile phase from 50% water (1% trifluoroacetic acid) and 50% acetonitrile (1% trifluoroacetic acid) to 100% acetonitrile.

b-DNA and mRNA production

b-DNAs were designed as previously described[31] and synthesized and purified by Integrated DNA Technologies (Supplementary Table 2). Briefly, the 61-nucleotide b-DNA sequence contained five phosphorothioate bonds at each end, with a ten-nucleotide barcode region in the centre. Another ten randomized nucleotides were included at the 3′ end of the barcode region, and the 5′ and 3′ ends of each b-DNA contained priming sites for the addition of Illumina-compatible adapters.

Luciferase mRNA was synthesized by in vitro transcription (IVT) using Ambion's MEGAscript kit with linearized plasmids (pLuc19) encoding codon-optimized firefly luciferase and T7 RNA polymerase (ThermoFisher Scientific) as previously described[66]. mRNA was transcribed with the N^1-methyl-pseudouridine modification and 130-nucleotide-long poly(A) tails[67]. RNA was capped using a ScriptCap m^7G capping kit with 2′-*O*-methyltransferase (CellScript) to obtain the cap previously described as cap1 (ref. 67). Finally, mRNA was purified by fast protein liquid chromatography using an Akta purifier (GE Healthcare) as previously described[68]. mRNA product integrity was validated using denaturing or native agarose gel electrophoresis, and mRNA was stored frozen for later use.

For VEGF mRNA production, a double-stranded DNA IVT template was purchased (Integrated DNA Technologies) as a gBlock consisting of a T7 RNA polymerase promoter, a 5′ untranslated region derived from tobacco etch virus, a mouse codon-optimized $VEGF_{164}$-A coding sequence and a 3′ untranslated region derived from *Xenopus* beta globin. The template was amplified by PCR with Q5 High-Fidelity DNA Polymerase (New England BioLabs; NEB) and purified using Monarch PCR & DNA Cleanup spin columns (NEB). IVT was performed using a HiScribe T7 High Yield RNA Synthesis kit (NEB), and full N^1-methyl-pseudouridine substitution was achieved by replacing UTP with N^1-methylpseudouridine-5′-triphosphate (TriLink Biotechnologies). Cotranscriptional capping was achieved using a CleanCap Reagent AG cap1 analogue (TriLink Biotechnologies). RNA was purified using Monarch RNA Cleanup spin columns (NEB). RNA transcripts were polyadenylated using *Escherichia coli* poly(A) polymerase (NEB) and purified once again using RNA Cleanup spin columns. mRNA product integrity was validated using native agarose gel electrophoresis and mRNA was stored frozen for later use.

LNP formulation and characterization

A library of 98 LNPs was formulated using a 10:1 molar ratio of ionizable lipid to nucleic acid with a unique ionizable lipid and excipient formulation[38] (Supplementary Table 1). For all LNPs excluding LNP 98, the ionizable lipid was combined in an ethanol phase with cholesterol (MilliporeSigma), 1,2-dioleoyl-*sn*-glycero-3-phosphoethanolamine (Avanti Polar Lipids) and 1,2-dimyristoyl-*sn*-glycero-3-phosphoethanolamine-*N*-[methoxy(polyethylene glycol)-2000] (ammonium salt) ($C14\text{-}PEG_{2000}$, Avanti Polar Lipids) to a total volume of 112.5 µl. For LNP 98, the ionizable lipid DLin-MC3-DMA was combined in an ethanol phase with cholesterol (MilliporeSigma), 1,2-distearoyl-*sn*-glycero-3-phosphocholine (Avanti Polar Lipids) and 1,2-dimyristoyl-rac-glycero-3-methoxypolyethylene glycol-2000 ($DMG\text{-}PEG_{2000}$, Avanti Polar Lipids) to 112.5 µl. For some formulations, C14-494 or 1,2-dioleoyl-*sn*-glycero-3-phospho-L-serine (Avanti Polar Lipids) was added to the LNP 98 formulation as a fifth component according to molar ratios reported previously[20].

A separate aqueous phase was prepared with 25 µg of b-DNA, luciferase mRNA, β_2-GPI siRNA or VEGF mRNA in 10 mM citrate buffer to a total volume of 337.5 µl. For high-throughput screening with b-DNA, ethanol and aqueous phases were combined by pipette mixing to form LNPs[31,69]. For luciferase mRNA, β_2-GPI siRNA and VEGF mRNA LNPs, ethanol and aqueous phases were combined by chaotic mixing using a microfluidic device designed with herringbone features[70]. LNPs were dialysed against 1× PBS in either Pierce 96-well microdialysis plates or Slide-A-Lyzer dialysis cassettes with a molecular weight cutoff of 20 kDa (Thermo Fisher Scientific) for 2 h, sterilized using 0.22 µm filters and stored at 4 °C for later use.

For dynamic light scattering measurements, LNPs were diluted 10–100× in 1× PBS. Z-average diameter and polydispersity index were recorded using either a Zetasizer Nano (Malvern Panalytical) or using a DynaPro Plate Reader III (Wyatt Technology). For zeta potential measurements, 20 µl of LNP was diluted 50× in ultrapure water in disposable folded capillary cells and measured using a Zetasizer Nano. For high-throughput screening, z-average diameter, polydispersity index and zeta potential are reported as the mean ($n = 3$ measurements for each sample) (Supplementary Table 3).

b-DNA and RNA encapsulation efficiencies for each LNP formulation were measured using a Quant-iT-OliGreen (Thermo Fisher Scientific) assay and Quant-iT-RiboGreen (ThermoFisher Scientific) assay, respectively. Each LNP sample was diluted 100× in either 1× Tris-EDTA (TE) buffer or TE buffer containing 0.1% (v/v) Triton X-100 (MilliporeSigma). LNPs in TE buffer, LNPs in Triton X-100 and standards were plated in black 96-well plates, and either the OliGreen or RiboGreen fluorescence detection reagent was added to each well per the manufacturer's instructions. Fluorescence intensity was measured using an Infinite 200 Pro plate reader (Tecan). Encapsulated b-DNA and RNA were estimated by comparison with a standard curve fitted using univariate least-squares linear regression. Encapsulation efficiency was calculated as $(B - A)/B \times 100\%$, where A is the measured nucleic acid content in TE buffer and B is the measured nucleic acid content in Triton X-100. For high-throughput screening, encapsulation efficiency is reported as the mean ($n = 4$ measurements for each sample) (Supplementary Table 3).

The pK_a, or pH at which the LNP is 50% protonated, was measured for various LNP formulations as previously described[71]. Briefly, a buffered solution containing 150 mM sodium chloride, 20 mM sodium phosphate, 20 mM ammonium acetate and 25 mM ammonium citrate was

pH-adjusted to generate solutions from pH 2.0 to 12.0 in increments of 0.5. Then, 125 µl of each pH-adjusted solution and 5 µl of each LNP were plated in quadruplicate in black 96-well plates, and 6-(*p*-toluidinyl) naphthalene-2-sulfonic acid was added to each well to a final concentration of 6 µM. Fluorescence intensity was read on an Infinite 200 Pro plate reader (Tecan) with excitation/emission wavelengths of 322/431 nm.

Animal experiments

All animal use was in accordance with the guidelines of and approval from the University of Pennsylvania's Institutional Animal Care and Use Committee (protocol number 806540). Non-pregnant 6–8-week-old female C57BL/6 mice and time-dated pregnant female C57BL/6 mice were purchased from Jackson Laboratory. Time-dated pregnancies were also achieved by housing four C57BL/6 females and one C57BL/6 male all at least 8–10 weeks of age together in one cage overnight and separating the male the next morning. Consistent with the breeding scheme established by Jackson Laboratory, separation was deemed to be gestational day E0. Pregnancies were confirmed visually on or after gestational day E11 or by measuring weight change. Mice were housed in a vivarium with a 12 h light–dark cycle and were provided with food and water ad libitum. Vivarium temperature and humidity were maintained between 68 and 76 °F and 30 and 70%, respectively.

b-DNA library preparation and next-generation sequencing

A constant volume of each of the 98 LNP formulations encapsulating a unique b-DNA oligomer was used to generate an injection pool, which was then combined with a naked, unencapsulated b-DNA oligo. Although no evidence of LNP aggregation in pooled LNP samples was observed (Supplementary Fig. 9d), the pooled LNPs were immediately (within 6 h) administered i.v. by tail vein injection to non-pregnant mice and gestational day E16 pregnant mice. Six hours following administration, mice were euthanized with CO_2, and the heart, lungs, liver, kidneys, spleen, uterus, fetuses and placentas were collected into SPEX 5 ml polyethylene vials with 9.5 mm steel grinding balls (SPEX Sample Prep) on dry ice. Organs were snap-frozen using liquid nitrogen, and a 2010 Geno/Grinder (SPEX Sample Prep) was used to generate powdered tissue homogenates by two consecutive homogenization cycles of 30 s at a speed of 750 strokes per min.

Approximately 50 mg of powdered tissue was weighed into 1.5 ml tubes and incubated in 750 µl of lysis buffer containing 100 mM Tris-HCl, 5 mM EDTA, 0.2% SDS, 200 mM NaCl and 0.2 mg ml^{-1} proteinase K (ThermoFisher Scientific) overnight at 37 °C. Then, 1 µl of 4 mg ml^{-1} RNase A (Promega) was added to each sample, followed by incubation for 1 h at 37 °C, and samples were centrifuged for 5 min at 15,000*g*. Oligos were extracted from 300 µl of sample supernatant using an Oligo Clean and Concentrator kit (Zymo Research) according to the manufacturer's instructions. PCR on eluted DNA was performed using Phusion High-Fidelity DNA Polymerase for 35 cycles (NEB). The list of full-length reverse primers (index sequences) can be found in Supplementary Table 13. The forward primer sequence was as follows: 5′-AATGATACGGCGACCACCGAGATCTACACTCTTTCCCTACACGACGCTCTTCCGATCT-3′.

PCR products were purified using gel electrophoresis with a 3% agarose gel (ThermoFisher Scientific) in Tris-acetate-EDTA running buffer (ThermoFisher Scientific). Amplified b-DNA was excised from the gel and purified using a Zymo Gel DNA Recovery kit (Zymo Research) according to the manufacturer's instructions. The pooled, uninjected library of LNP formulations was processed using the protocol described above and amplified with a unique reverse primer. The next-generation sequencing library was balanced and pooled using a Quant-iT-PicoGreen assay (ThermoFisher Scientific). Quality control was performed using an Agilent Bioanalyzer system to check library purity and measure concentration for loading the flow cell at a concentration of 4 nM. Next-generation sequencing was performed using multiplexed runs on an Illumina MiSeq.

Normalized delivery of a particular b-DNA LNP to a particular tissue was calculated as the ratio of two frequencies[31]. Briefly, within one tissue sample, the sequencing reads from each b-DNA were divided by the sum of reads from all b-DNAs in the tissue sample. Similarly, within the uninjected LNP pool, the sequencing reads from each b-DNA were divided by the sum of reads from all b-DNAs in the uninjected pool. Normalized delivery for each b-DNA to a particular tissue was calculated as the ratio of these two frequencies.

In vivo luciferase mRNA LNP delivery

LNPs encapsulating luciferase mRNA were administered i.v. to non-pregnant and gestational day E16 pregnant mice at doses of 0.6 or 1.0 mg kg^{-1} of mRNA. In some experiments, LNPs were labelled with 10 µM Vybrant DiD Cell-Labeling Solution (ThermoFisher Scientific) for 15 min at 25 °C with gentle shaking at 300 rpm. Six or twelve hours following administration, luminescence and/or DiD fluorescence imaging was performed using Living Image software on an IVIS (PerkinElmer). Ten minutes before imaging, D-luciferin potassium salt (Biotium) was administered i.p. to mice at a dose of 150 mg kg^{-1}. Mice were subsequently euthanized with CO_2, and the heart, lungs, liver, kidneys, spleen, fetuses and placentas were dissected and imaged.

For in vivo β_2-GPI siRNA-mediated knockdown experiments, on gestational day E13, pregnant mice were treated i.v. with 1 mg kg^{-1} of predesigned β_2-GPI siRNA (MilliporeSigma, SASI_Mm01_00_67354/APOH) encapsulated in the C12-200 LNP formulation. The siRNA sequences were as follows (where [dT] indicates a deoxythymidine residue): strand 1—5′-GUUUACCUGUCCUCUCACA[dT][dT]-3′ and strand 2—5′-UGUGAGAGGACAGGUAAAC[dT][dT]-3′.

Seventy-two hours later and immediately before i.v. administration of LNP 55 or 98, blood was collected retro-orbitally using non-heparinized capillary tubes (ThermoFisher Scientific) into Microtainer blood collection tubes (Becton, Dickinson and Company; BD). Blood was allowed to clot for 2 h at room temperature; it was then centrifuged for 20 min at 2000*g* to collect serum, which was subsequently stored at −20 °C for further analysis of β_2-GPI levels by ELISA (Novus Biologicals). Pregnant mice were treated i.v. with luciferase mRNA LNPs at a dose of 0.6 mg kg^{-1} of mRNA, and tissues were dissected and imaged as described above. To quantify luminescence, Living Image Software (PerkinElmer) was used to place a rectangular region of interest around the tissue of interest. The spleen-to-liver ratio was calculated by dividing the luminescence in the spleen by the luminescence in the liver.

In vitro luciferase mRNA LNP delivery and cellular uptake

The Hep G2 hepatocyte, Jurkat T cell, Raji B cell and RAW 264.7 macrophage cell lines were purchased from ATCC; and the BeWo b30 choriocarcinoma cell line was provided by D. Huh at the University of Pennsylvania. All cell lines tested negative for mycoplasma at the University of Pennsylvania's Cell Center. The morphology of all cells was checked at every subculture or passage to ensure they were free from contamination for authentication purposes. Hep G2, RAW 264.7 and BeWo b30 cells were cultured in Dulbecco's modified Eagle medium with L-glutamine (Gibco) supplemented with 10% (v/v) fetal bovine serum (Gibco) and 1% (v/v) penicillin–streptomycin (Gibco). Jurkat and Raji cells were cultured in Roswell Park Memorial Institute 1640 medium with L-glutamine (Gibco) with the same supplements.

For luciferase mRNA expression experiments, cells were plated in 96-well plates (ThermoFisher Scientific) at densities of 10,000 cells per 100 µl (Hep G2), 60,000 cells per 100 µl (Raji and Jurkat) or 20,000 cells per 100 µl (RAW 264.7 and BeWo b30). Hep G2, RAW 264.7 and BeWo b30 cells were plated and allowed to adhere overnight, and the medium was changed to Opti-MEM Reduced Serum Medium (Gibco) before treatment. Luciferase mRNA LNPs were incubated with either

recombinant human ApoE4 (ThermoFisher Scientific) or recombinant mouse β_2-GPI (ThermoFisher Scientific) at doses of 0, 0.1, 0.25, 0.5, 0.75 and 1 μg of protein per μg of lipid for 15 min at 37 °C with gentle shaking at 300 rpm. Hep G2 cells were treated with 5 ng of encapsulated luciferase mRNA, while Jurkat, Raji, RAW 264.7 and BeWo b30 cells were treated with 20 ng of encapsulated luciferase mRNA. Twenty-four hours after LNP treatment, medium was removed, and 50 μl 1× reporter lysis buffer (Promega) was added to each well, followed by 100 μl luciferase assay substrate (Promega). After 10 min of incubation, luminescence intensity was quantified using an Infinite 200 Pro plate reader (Tecan). For in vitro protein adsorption assays, normalized luciferase expression was calculated first by subtracting the luminescence signal from untreated cells and then dividing by the mean luminescence signal from cells treated with uncoated (no protein) LNPs. For in vitro shelf-life assays, normalized luciferase expression was calculated first by subtracting the luminescence signal from wells containing untreated cells and then dividing by the mean luminescence signal from cells treated with an equivalent amount of RNA (20 ng) freshly prepared with Lipofectamine MessengerMAX (Thermo Fisher Scientific).

For cellular uptake evaluations using confocal microscopy, Hep G2, Jurkat and BeWo b30 cells were plated in Nunc Lab-Tek II four chamber slides (ThermoFisher Scientific) at densities of 200,000 cells per ml (Hep G2 and BeWo b30) or 400,000 cells per ml (Jurkat). Hep G2 and BeWo b30 cells were plated and allowed to adhere overnight, and the medium was changed to Opti-MEM Reduced Serum Medium before treatment. For Jurkat cells, chambers were coated with 50 μg ml^{-1} poly-L-lysine (MilliporeSigma) in 10 mM Tris-HCl (ThermoFisher Scientific) for 30 min and then allowed to dry overnight. DiD-labelled luciferase mRNA LNPs were incubated with either recombinant human ApoE4 or recombinant mouse β_2-GPI at doses of 0 or 0.75 μg of protein per μg of lipid for 15 min at 37 °C with gentle shaking at 300 rpm. Hep G2, Jurkat, and BeWo b30 cells were treated with 200 ng of encapsulated luciferase mRNA. Thirty minutes after treatment, medium was removed, and cells were washed with 1× PBS and fixed with 4% paraformaldehyde (MilliporeSigma) for 15 min. Cells were then washed with 1× PBS and counterstained with 1 μg ml^{-1} DAPI (ThermoFisher Scientific) for 5 min. Finally, slides were mounted to glass coverslips (ThermoFisher Scientific) with ProLong Diamond Antifade Mountant (ThermoFisher Scientific) overnight before imaging. Slides were imaged using a Leica Stellaris 5 confocal laser scanning microscope equipped with a fixed 405 nm DAPI laser and an extended tuneable white light laser with a ×20 objective.

For cellular uptake evaluations using flow cytometry, Hep G2, Jurkat and BeWo b30 cells were plated in 96-well plates at a density of 50,000 cells per 100 μl. Hep G2 and BeWo b30 cells were plated and allowed to adhere overnight, and the medium was changed to Opti-MEM Reduced Serum Medium before treatment. Luciferase mRNA LNPs were labelled with DiD and coated with protein as described above and used to treat Hep G2, Jurkat and BeWo b30 cells with 50 ng of encapsulated luciferase mRNA. Thirty minutes after LNP treatment, medium was removed, and cells were washed with 1× PBS with 2 mM EDTA. Single-cell suspensions were analysed by flow cytometry for DiD fluorescence intensity using Luminex InCyte software on a Guava easyCyte flow cytometer equipped with blue, green and red lasers (Luminex). At least 10,000 events corresponding to singlets were acquired for all experimental samples. The percentage of DiD$^+$ cells is reported as mean ± s.e.m. (n = 4 biological replicates with n = 6 technical replicates each).

In vivo LNP delivery to splenic and placental cells

Spleens and placentas were collected into 2 ml of ultrapure H_2O and placed on ice for subsequent cell isolation and staining for flow cytometric analysis[58]. Briefly, the tissues were passed through 100 μm cell strainers (MilliporeSigma) to generate cell suspensions. Placenta cell suspensions were treated with 1% (v/v) 2000 U/mL DNase I (NEB) and 10% (v/v) 10X DNase I buffer (NEB) for 30 min at room temperature. Ammonium-chloride-potassium (ACK) lysis buffer (ThermoFisher Scientific) was then added to spleen and placenta cell suspensions for 5 min, cells were centrifuged at 500g for 5 min and the supernatant was removed. ACK lysis was repeated until red blood cells were removed, and the resulting pellet was resuspended in 1× PBS with 2 mM EDTA. Then, 0.5 μl of TruStain FcX PLUS (anti-mouse CD16/32) antibody (BioLegend) was added to each sample for 10 min at 4 °C.

Spleen samples were stained for cell surface markers for 30 min at 4 °C with 5 μl Brilliant Violent 421 anti-mouse CD45 antibody, 5 μl Brilliant Violet 711 anti-mouse CD19 antibody, 2 μl FITC anti-mouse CD3 antibody, 2 μl PE anti-mouse CD11c antibody and 5 μl PE-Cyanine7 anti-mouse CD11b antibody (BioLegend). Placenta samples were stained for cell surface markers for 30 min at 4 °C with 3 μl Brilliant Violet 421 anti-mouse CD45 antibody and 1.5 μl FITC anti-mouse CD31 antibody (BioLegend). Placenta samples were then washed, fixed and permeabilized using a Cyto-Fast Fix/Perm buffer kit (BioLegend) per the manufacturer's instructions. Placental cells were then stained intracellularly with 3 μl PE anti-mouse cytokeratin 7 antibody (Novus Biologicals). Data were acquired using BD FACSDiva software on a BD LSR II flow cytometer equipped with violet, blue, green and red lasers. At least 50,000 events corresponding to singlets were acquired for all samples. Thresholds for positivity were determined using fluorescence-minus-one controls (Supplementary Figs. 21 and 22).

Placentas were also collected for immunofluorescence analysis; after dissection, placentas were immediately placed in 10% neutral buffered formalin (MilliporeSigma) for twenty-four hours. Samples were then dehydrated in ethanol, embedded in paraffin wax and sectioned into 4-μm-thick sections longitudinally from the centre of the placenta. Sections were then stained for cytokeratin 7 (primary: rabbit anti-mouse cytokeratin 7 antibody (1:200, Abcam); secondary: PE donkey anti-rabbit antibody (1:200, BioLegend)) or endomucin (primary: goat anti-mouse endomucin antibody (1:200, R & D Systems; secondary: FITC donkey anti-goat antibody (1:200, Abcam)) and counterstained with DAPI. Slides were then mounted to coverslips, after which images were acquired using the Leica Application Suite X on a Leica Stellaris 5 confocal laser scanning microscope with a ×20 objective. Images were collected for two placentas per mouse, two sections per placenta and three images per section with reproducible results.

Inflammation- and hypoxia-induced pre-eclampsia models

For inflammation-induced pre-eclampsia, time-dated pregnant mice arrived on gestational day E5 and were randomly allocated into three cohorts; on E7, 200 μl of either 1× PBS or 1 μg kg^{-1} LPS (MilliporeSigma) was administered i.p.[55–57]. For hypoxia-induced pre-eclampsia, females at least 8–10 weeks of age were ear-tagged and weighed before timed-dated pregnancies were set up as described above. On gestational day E7, female mice were weighed, and those with a change in body weight of at least 1.5 g were randomly allocated into five cohorts. Pregnant mice were then treated i.v. with 1×10^9 PFU of Adv-sFlt-1 (refs. 6,61) (Vector BioLabs) diluted in 1× PBS. For both the inflammation- and hypoxia-induced models of pre-eclampsia, on gestational day E11, LNP 55 or 98 encapsulating VEGF mRNA was administered i.v. to mice at a dose of 1 mg kg^{-1} of mRNA.

Mice were weighed daily from gestational day E6 to E16, and daily weight change was calculated for gestational days E7 to E16 by subtracting the initial body weight measurement from E6. Pregnant mice were trained using a CODA Monitor Noninvasive Blood Pressure System (Kent Scientific Corporation) on gestational days E5 and E6 before recording a preliminary blood pressure reading on E7. Maternal mean arterial pressure was recorded daily at the same time of day from E7 to E16; two to four readings were recorded for each mouse per day.

On gestational days E11.5 (six hours following LNP treatment) and E17, blood was collected retro-orbitally for serum analysis as described above. Similarly, at the study end point, blood was collected

retro-orbitally in 1.5 ml tubes prefilled with 200 µl 0.5 M EDTA for flow cytometric analysis. Urine was also collected at the study end point by applying firm but gentle pressure to the lower backs of the mice to expel urine from the bladder onto a clean plastic surface. Urine was transferred to tubes for storage at −20 °C for further analysis. Mice were then euthanized with CO_2, and fetuses, placentas, kidneys and spleens were dissected. Fetuses and placentas were weighed individually with a precision balance (Mettler Toledo, Columbus, OH). Total litter weight was calculated for each mouse as the sum of the weights of all fetuses in the litter.

Spleens and placentas were prepared for flow cytometric analysis as described above. Similarly, blood was prepared by several rounds of red blood cell lysis using ACK lysis buffer until cell pellets were clear. Blood and spleen cell pellets were resuspended in 1× PBS with 1% bovine serum albumin, and placenta cell pellets were resuspended in 1× PBS with 2 mM EDTA. Then, 0.5 µl of TruStain FcX PLUS (anti-mouse CD16/32) antibody (BioLegend) was added to each sample for 10 min at 4 °C. Blood, spleen and placenta cell samples were stained for surface markers for 30 min at 4 °C with 1 µl Spark 387 anti-mouse CD8 antibody, 2 µl Brilliant Violet 421 anti-mouse CD4 antibody, 2 µl Brilliant Violet 711 anti-mouse CD19 antibody, 2 µl PerCP anti-mouse CD45 antibody, 2 µl PE anti-mouse CD25 antibody, 2 µl PE-Cy7 anti-mouse CD11b antibody, 1 µl AlexaFluor 700 anti-mouse CD11c antibody and 2 µl APC anti-mouse CD3 antibody (BioLegend). Data were acquired using BD FACSDiva software on a BD LSRFortessa flow cytometer equipped with ultraviolet, violet, blue, yellow/green and red lasers. At least 50,000 events corresponding to singlets were acquired for all spleen and placenta samples, and at least 10,000 events corresponding to singlets were acquired for blood samples. Thresholds for positivity were determined using fluorescence-minus-one controls (Supplementary Fig. 25).

Placentas and kidneys were prepared for histological sectioning as described above and stained using H&E. An EVOS FL Auto 2 wide-field microscope (ThermoFisher Scientific) was used to image H&E-stained placenta and kidney sections. Mean blood vessel area in the labyrinth region of the placenta was calculated as previously described[23]. Briefly, two H&E-stained sections were prepared for each placenta, and three images were taken in the labyrinth region for each section. The Analyze Particles tool in ImageJ was used to calculate the mean vessel area for each image.

Mouse Quantikine ELISA kits (R & D systems) were used to evaluate VEGF, sFlt-1, TNF, IL-6 and IFNγ levels in serum per the manufacturer's instructions. Colorimetric assay kits (Cayman Chemical) were used to evaluate ALT and AST levels in serum per the manufacturer's instructions. Fluorescence assay kits (Abcam) were used to evaluate urine albumin concentration per the manufacturer's instructions.

Statistical analysis

All plots were generated using RStudio or GraphPad Prism. FlowJo was used to analyse flow cytometry data. ImageJ2 was used to analyse wide-field microscopy and confocal laser scanning microscopy images. Data in normalized delivery heatmaps represent the mean, and data in violin plots (for instance, for fetal and placental weight, mean blood vessel area) represent the median with the 25th and 75th percentiles. All other data are presented as the mean ± s.e.m. with the exact number of replicates reported in the figure legends. All samples had at least $n = 3$ biological replicates, and no statistical methods were used to predetermine sample size. Investigators were not blinded during outcome assessment or data analysis.

Ordinary (one technical replicate per biological replicate) or nested (multiple technical replicates per biological replicate) two-sided, one-way analyses of variance (ANOVAs) with post hoc Student's *t*-tests using the Holm–Šídák correction for multiple comparisons were used to compare responses across treatment groups. Each fetus or placenta from one mouse was considered a technical replicate. Two-sided ordinary two-way ANOVAs with post hoc Student's *t*-tests using the Holm–Šídák correction for multiple comparisons were used to compare responses across treatment groups and gestational days or mouse cohorts (non-pregnant versus pregnant). For data with only two treatment groups, either ordinary or nested unpaired, two-tailed Student's *t*-tests were used to compare responses across treatment groups. To generate volcano plots, ordinary two-sided, one-way ANOVAs with post hoc Student's *t*-tests using the Holm–Bonferroni correction for multiple comparisons were used to compare normalized LNP delivery with the C12-200 formulation.

Least-squares linear regression was used to calculate the pK_a (reported with 95% confidence interval), defined as the pH corresponding to half-maximum fluorescence intensity. To generate correlation coefficient heatmaps, the squared Pearson's correlation coefficient of mean normalized delivery was calculated for each pair of organs. Least-squares multiple linear regression models of normalized b-DNA delivery to proximal and distal placentas as well as encapsulation efficiency were constructed. Linear models were stepwise simplified on the basis of the Akaike information criterion to identify key parameters influencing placental b-DNA delivery and encapsulation.

Reporting summary

Further information on research design is available in the Nature Portfolio Reporting Summary linked to this article.

Data availability

Demultiplexed next-generation sequencing data from b-DNA LNP screening are available at https://upenn.box.com/v/VEGF-LNPs-preeclampsia. Source data are provided with this paper.

Code availability

Supplementary Code 1 for read extraction and tabulation and Supplementary Code 2 for data transformation/normalization are provided with this paper.

66. Pardi, N., Muramatsu, H., Weissman, D. & Karikó, K. in *Synthetic Messenger RNA and Cell Metabolism Modulation: Methods and Protocols* Vol. 969 (ed. Rabinovich, P. M.) 29–42 (Humana, 2013).
67. Karikó, K. et al. Incorporation of pseudouridine into mRNA yields superior nonimmunogenic vector with increased translational capacity and biological stability. *Mol. Ther.* **16**, 1833–1840 (2008).
68. Weissman, D., Pardi, N., Muramatsu, H. & Karikó, K. in *Synthetic Messenger RNA and Cell Metabolism Modulation: Methods and Protocols* (ed. Rabinovich, P. M.) 43–54 (Humana, 2013).
69. Zhang, R. et al. Helper lipid structure influences protein adsorption and delivery of lipid nanoparticles to spleen and liver. *Biomater. Sci.* **9**, 1449–1463 (2021).
70. Chen, D. et al. Rapid discovery of potent siRNA-containing lipid nanoparticles enabled by controlled microfluidic formulation. *J. Am. Chem. Soc.* **134**, 6948–6951 (2012).
71. Hajj, K. A. et al. Branched-tail lipid nanoparticles potently deliver mRNA in vivo due to enhanced ionization at endosomal pH. *Small* **15**, 1805097 (2019).

Acknowledgements M.J.M. acknowledges support from a US National Institutes of Health (NIH) Director's New Innovator Award (DP2 TR002776), a Burroughs Wellcome Fund Career Award at the Scientific Interface (CASI), a US National Science Foundation CAREER Award (CBET-2145491) and the NIH (NICHD R01 HD115877). K.L.S., A.G.H., H.C.S., H.C.G., A.S.T., A.M.M., E.L.H. and A.J.M. acknowledge support from the US National Science Foundation Graduate Research Fellowship. R.P. was supported by an NIH National Heart, Lung, and Blood Institute Ruth L. Kirschstein Pre-Doctoral National Research Service Award. We thank the Next-Generation Sequencing Core at the University of Pennsylvania (RRID:SCR_022382) for assistance with next-generation sequencing. Data for this manuscript were generated in the Penn Cytomics and Cell Sorting Shared Resource Laboratory at the University of Pennsylvania (RRID:SCR_022376), which was partially supported by an Abramson Cancer Center NCI Grant (P30 016520). We also thank the Cell and Development Biology Microscopy Core at the University of Pennsylvania for access to the confocal laser scanning microscope used in this work (RRID:SCR_022373), and F. Chen from the Histotechnology Facility at the Wistar Institute for preparing histological samples for this work. Funding support for the Wistar Institute core facilities was provided by a Cancer Center Support Grant (P30 CA010815).

Author contributions K.L.S. and M.J.M. contributed to conceptualization, writing of the original draft and project administration. K.L.S., A.G.H., and M.J.M. contributed to the methodology and review and editing of the paper. K.L.S. and A.G.H. contributed to software and/or code and formal data analysis. K.L.S., A.G.H., H.C.S., H.C.G., A.S.T., R.P., A.M.M., E.L.H.,

A.J.M., X.H., R.A.J. and A.A.G. contributed to investigation. M.-G.A. and D.W. contributed resources. M.J.M. was responsible for supervision and funding acquisition.

Competing interests K.L.S., H.C.S., H.C.G. and M.J.M. have filed a patent application based on this work. M.J.M. is an inventor on a patent related to this work filed by the Trustees of the University of Pennsylvania (PCT/US20/56252). D.W. is an inventor on several patents related to this work filed by the Trustees of the University of Pennsylvania (11/990,646; 13/ 585,517; 13/839,023; 13/839,155; 14/456,302; 15/339,363; 16/299,202). The remaining authors declare no competing interests.

Additional information

Supplementary information The online version contains supplementary material available at https://doi.org/10.1038/s41586-024-08291-2.

Correspondence and requests for materials should be addressed to Michael J. Mitchell.

Peer review information *Nature* thanks Hideyoshi Harashima, Roy van der Meel and the other, anonymous, reviewer(s) for their contribution to the peer review of this work. Peer reviewer reports are available.

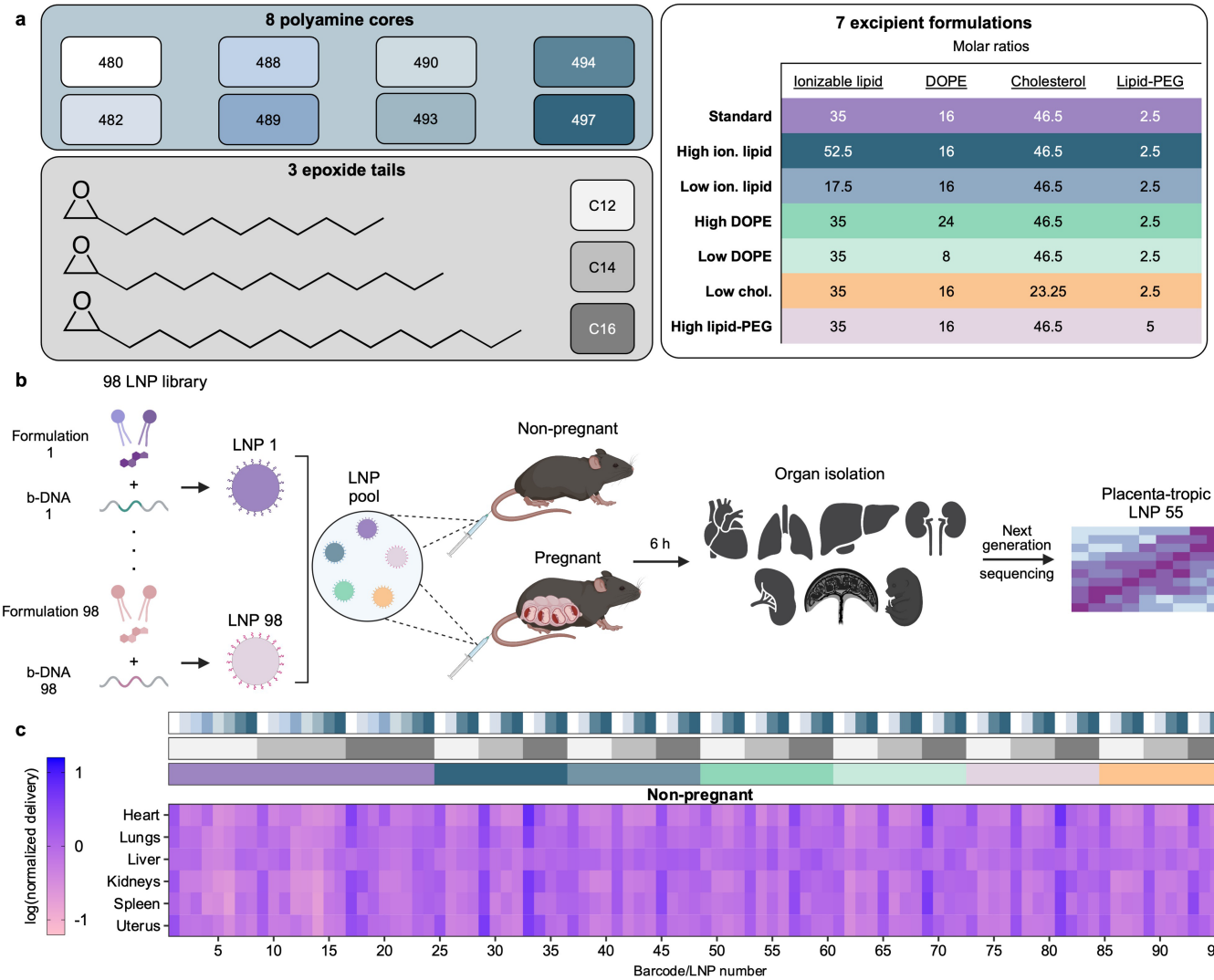

Extended Data Fig. 1 | High-throughput in vivo evaluation of a 98 LNP library using molecular barcoding in non-pregnant and pregnant mice. **a**, A large library of 98 LNP formulations was designed by synthesizing 24 unique ionizable lipid structures from 8 polyamine cores and 3 epoxide tails. 12 of these ionizable lipids were then further explored to formulate LNPs of varied excipient composition. **b**, Each of the 98 LNPs was formulated encapsulating a unique DNA barcode (b-DNA) to enable high-throughput, in vivo screening. The pooled LNPs were administered i.v. to non-pregnant and pregnant mice ($n = 6$ biological replicates) following which tissues were collected, processed, and prepared for next generation sequencing. Demultiplexing and subsequent data analysis identified a placenta-tropic LNP formulation. **c**, Heatmap depicting relative accumulation for each LNP/b-DNA in non-pregnant mouse tissues. Ion., ionizable; chol., cholesterol. Illustrations in **b** were created using BioRender (https://biorender.com).

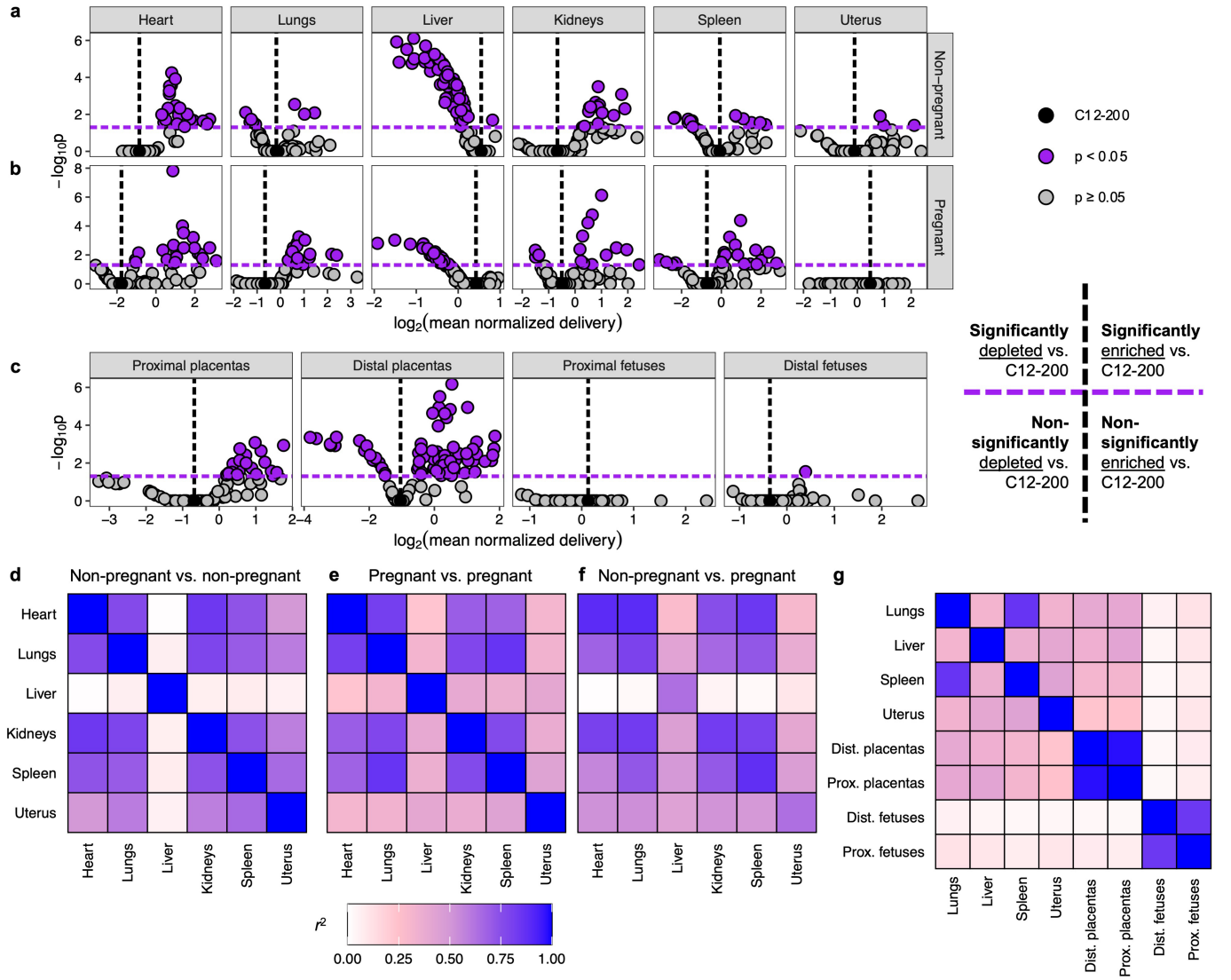

Extended Data Fig. 2 | Enrichment and correlation analysis of b-DNA LNP delivery in non-pregnant and pregnant mice. a–c, Volcano plots depicting significantly enriched (top right quadrant) and significantly depleted (top left quadrant) LNPs compared with the liver-tropic C12-200 LNP formulation in (**a**) non-pregnant and (**b**) pregnant tissues as well as (**c**) placentas and fetuses. Normalized delivery is reported as the mean ($n = 6$ biological replicates). For each tissue, two-sided, one-way ANOVAs with post hoc Student's *t* tests using the Holm-Bonferroni correction for multiple comparisons with the C12-200 LNP were used to compare normalized delivery across LNP formulations for generating *p* values. **d–g**, The squared Pearson's correlation coefficient for mean normalized delivery (r^2) was calculated for each tissue pair and is presented as a heatmap for (**d**) non-pregnant mouse tissues, (**e**) pregnant mouse tissues, (**f**) between non-pregnant and pregnant mouse tissues, and (**g**) between pregnant mouse tissues and the placentas and fetuses. Dist., distal; Prox., proximal.

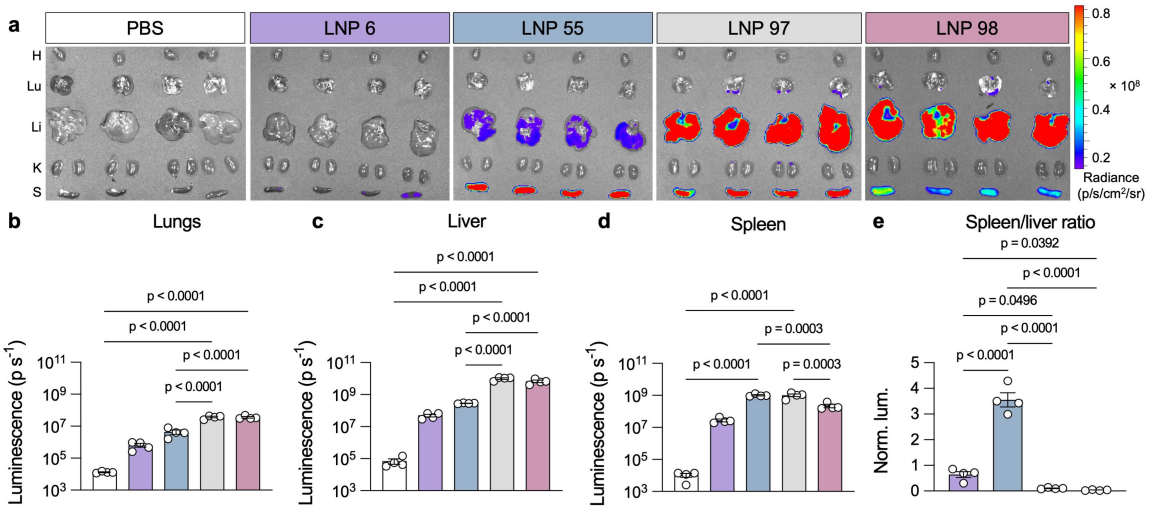

Extended Data Fig. 3 | Validation of results from high-throughput screening via luciferase mRNA delivery in non-pregnant mice. LNP 6 (negative control), LNP 55 (placenta-tropic), LNP 97 (C12-200), and LNP 98 (DLin-MC3-DMA) were formulated with luciferase mRNA and administered to non-pregnant mice at a dose of 0.6 mg kg^{-1} mRNA. **a**, Six hours after administration, tissues (H: heart, Lu: lungs, Li: liver, K: kidneys, S: spleen) were dissected and imaged using an in vivo imaging system (IVIS). **b**–**e**, Luminescence was quantified in the (**b**) lungs, (**c**) liver, and (**d**) spleen which was then used to calculate (**e**) a spleen-to-liver ratio. Luminescence measurements are reported as the mean ± s.e.m. ($n = 4$ biological replicates). Ordinary two-sided, one-way ANOVAs with post hoc Student's t tests using the Holm-Šídák correction for multiple comparisons were used to compare luminescence across treatment groups.

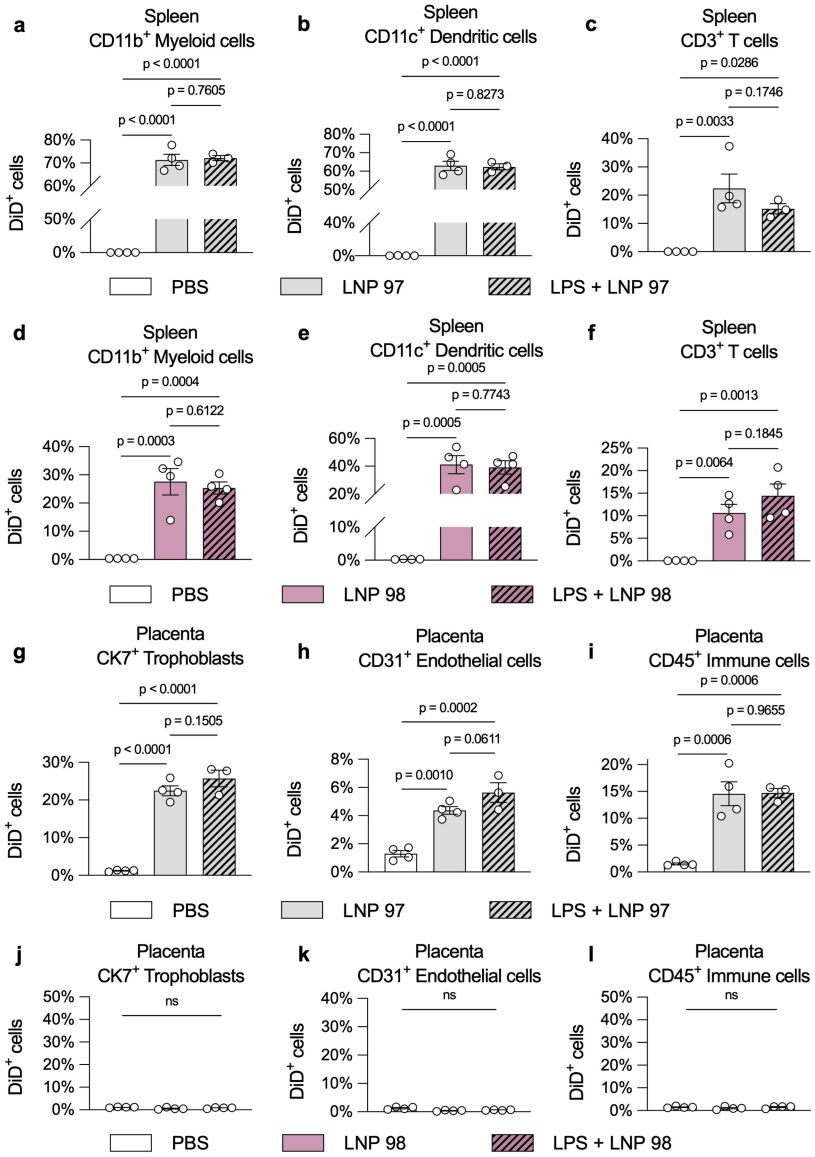

Extended Data Fig. 4 | Cellular LNP delivery in the spleen and placenta for industry and clinical standard LNPs in healthy and inflammation-induced pre-eclamptic mice. To evaluate differences in biodistribution between healthy and pre-eclamptic pregnant mice, inflammation-induced pre-eclampsia was established via i.p. administration of 1 μg kg^{-1} lipopolysaccharide (LPS). DiD-labelled LNPs 97 and 98 were administered at an mRNA dose of 1 mg kg^{-1}. Twelve hours later, cellular LNP delivery was evaluated in the (**a**–**f**) spleen and (**g**–**l**) placenta via flow cytometry. The percentage of DiD$^+$ cells is reported as the mean ± s.e.m. (PBS, LNP 97, LNP 98, LPS + LNP 98: $n = 4$ biological replicates; LPS + LNP 97: $n = 3$ biological replicates). Either ordinary (**a**–**f**) or nested (**g**–**l**) two-sided, one-way ANOVAs with post hoc Student's t tests using the Holm-Šídák correction for multiple comparisons were used to compare the percentage of DiD$^+$ cells across treatment groups. CK7: cytokeratin 7.

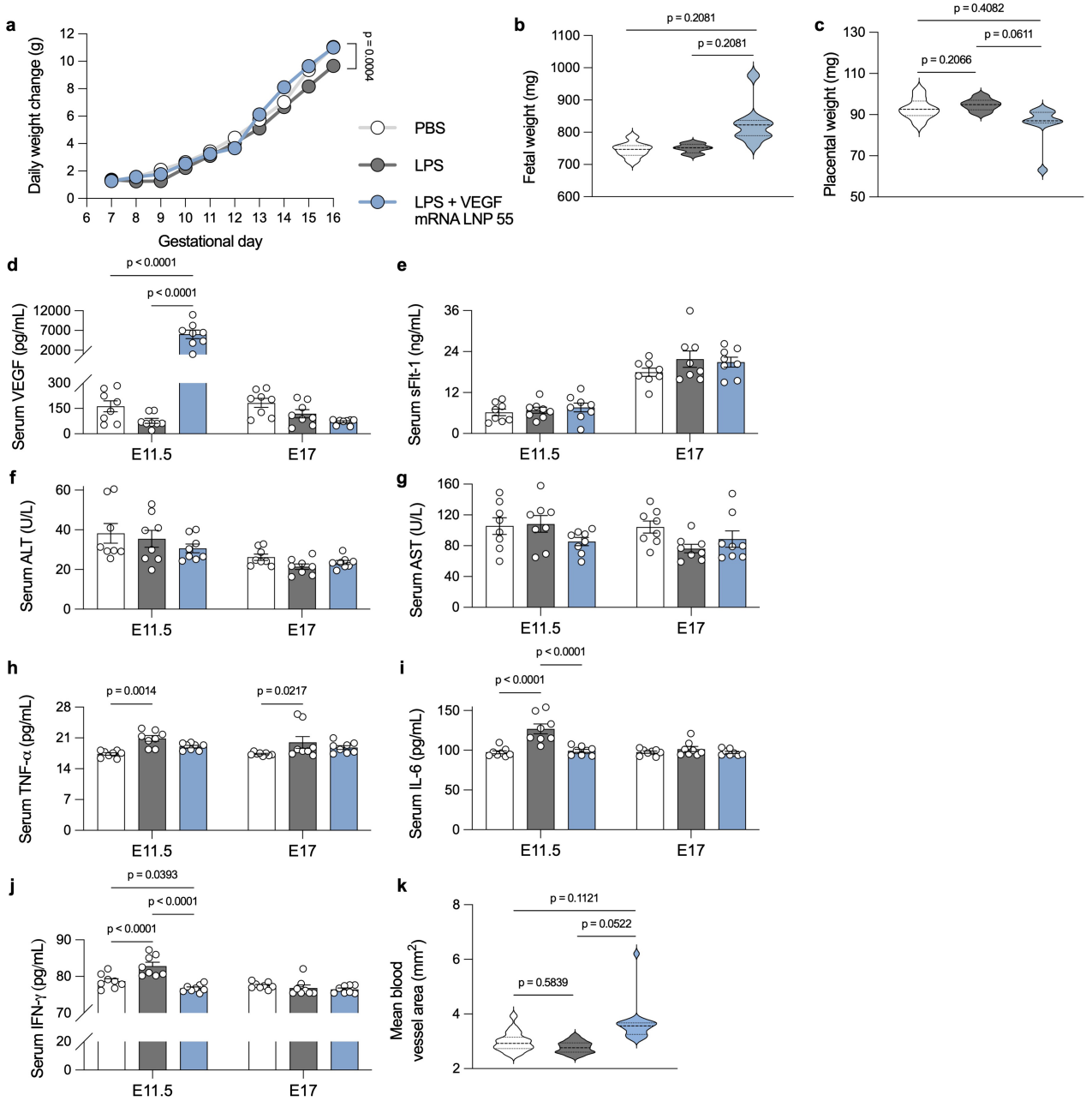

Extended Data Fig. 5 | VEGF mRNA LNP 55 improves maternal weight and serum concentration of inflammatory cytokines in inflammation-induced pre-eclampsia. Inflammation-induced pre-eclampsia was established through i.p. administration of 1 μg kg^{-1} lipopolysaccharide (LPS) on gestational day E7.5. 1 mg kg^{-1} VEGF mRNA LNP 55 was then administered i.v. on gestational day E11. **a**–**c**, Change in maternal weight was measured daily (**a**), and on gestational day E17 (**b,c**) fetal and placental weight were recorded. **d**–**j**, Serum levels of (**d**) VEGF, (**e**) sFlt-1, (**f**) alanine transaminase (ALT), (**g**) aspartate aminotransferase (AST), (**h**) tumour necrosis factor (TNF), (**i**) interleukin-6 (IL-6), and (**j**) interferon-γ (IFNγ) were evaluated on gestational days E11.5 and E17. **k**, Mean blood vessel area in the placental labyrinth was quantified from H&E-stainined placental sections. Maternal weight change and serum protein levels are reported as the mean ± s.e.m. ($n = 8$ biological replicates). Fetal and placental weight are reported as the median with the 25th and 75th percentiles ($n = 8$ biological replicates, 6–9 fetuses or placentas per mouse). Mean blood vessel area is reported as the median with the 25th and 75th percentiles ($n = 8$ biological replicates, 1–2 placentas per mouse, 2 sections per placenta, 2–3 images per section). Ordinary two-sided, two-way (**a, d**–**j**) or nested two-sided, one-way (**b**–**c, k**) ANOVAs with post hoc Student's *t* tests using the Holm-Šídák correction for multiple comparisons were used to compare responses across treatment groups.

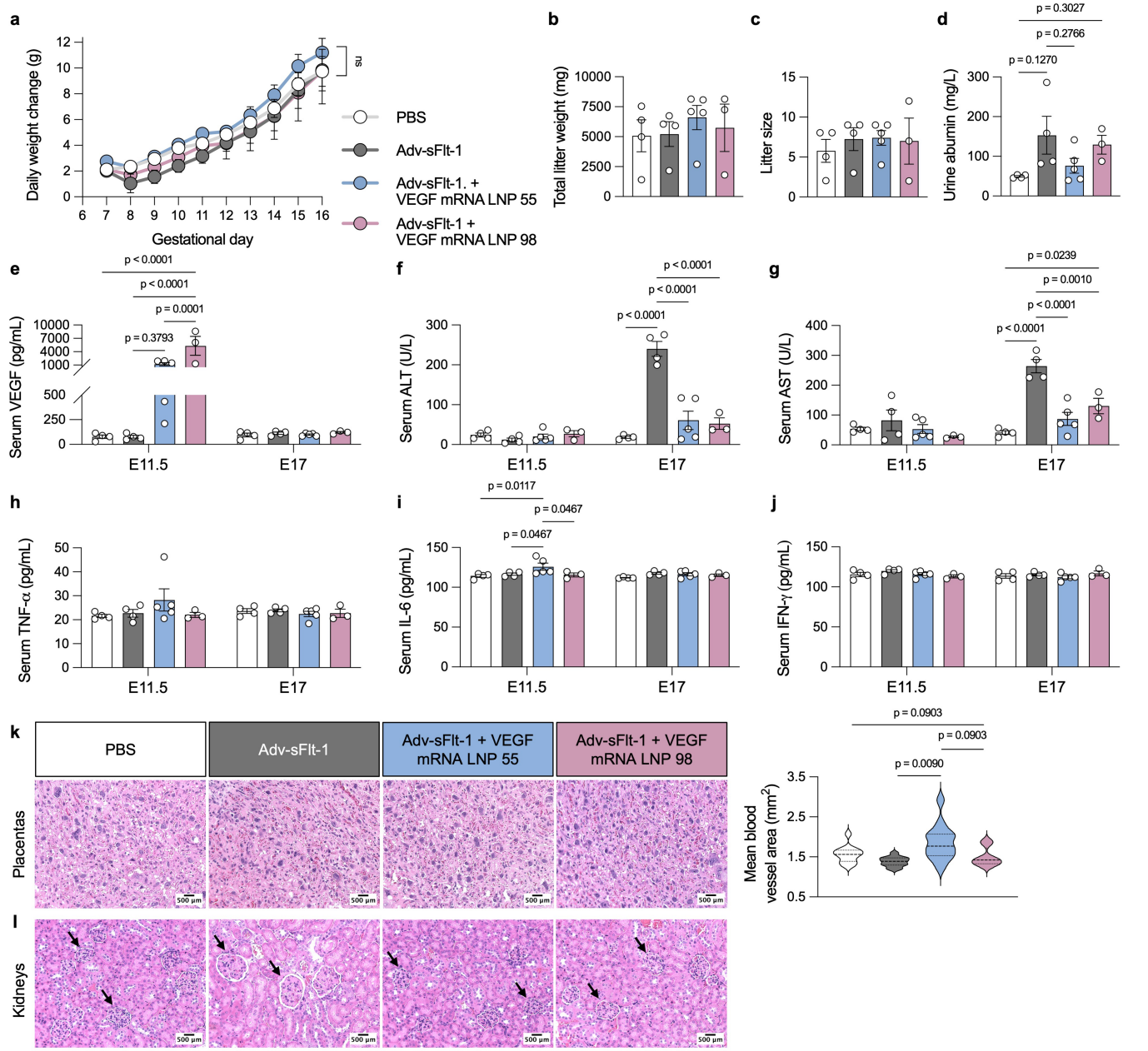

Extended Data Fig. 6 | VEGF mRNA LNP 55 reduces liver enzyme levels in serum and improves placental blood vessel area in hypoxia-induced pre-eclampsia. Hypoxia-induced pre-eclampsia was established through i.v. administration of 1×10^9 plaque forming units (PFU) of soluble Fms-like tyrosine kinase-1 adenovirus (Adv-sFlt-1) on gestational day E7.5. 1 mg kg^{-1} VEGF mRNA LNPs 55 or 98 were then administered i.v. on gestational day E11. **a**–**d**, Maternal weight change was recorded daily (**a**), and on gestational day E17 (**b**) total litter weight, (**c**) litter size, and (**d**) albumin concentration in urine were measured. **e**–**j**, Serum levels of (**e**) VEGF, (**f**) alanine transaminase (ALT), (**g**) aspartate aminotransferase (AST), (**h**) tumour necrosis factor (TNF), (**i**) interleukin-6 (IL-6), and (**j**) interferon-γ (IFNγ) were evaluated on gestational days E11.5 and E17. **k**, Placental vasculature in the labyrinth was visualized with H&E staining; stained sections were used to quantify mean blood vessel area. **l**, Similarly, renal histology was visualized using H&E staining with arrows indicating glomeruli. Maternal weight change, total litter weight, litter size, urine albumin concentration, and serum protein levels are reported as the mean ± s.e.m. (Adv-sFlt-1 + VEGF mRNA LNP 55: $n = 5$ biological replicates; PBS, Adv-sFlt-1: $n = 4$ biological replicates; Adv-sFlt-1 + VEGF mRNA LNP 98: $n = 3$ biological replicates). Mean blood vessel area is reported as the median with the 25th and 75th percentiles (1–2 placentas per mouse, 2 sections per placenta, 2–3 images per section). Ordinary (**b**–**d**) or nested (**k**) two-sided, one-way ANOVAs or ordinary two-sided, two-way ANOVAs (**a**, **e**–**j**) with post hoc Student's *t* tests using the Holm-Šídák correction for multiple comparisons were used to compare responses across treatment groups.

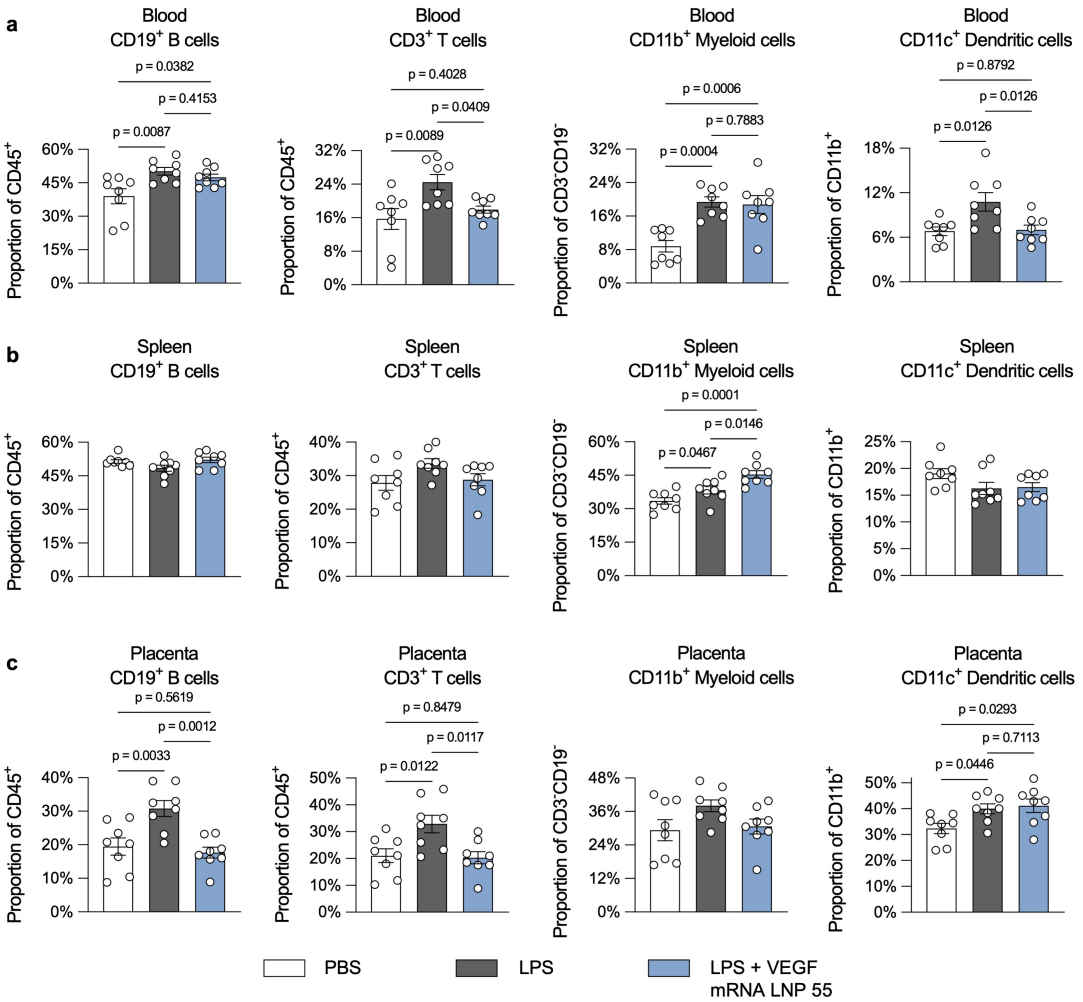

Extended Data Fig. 7 | In inflammation-induced pre-eclampsia, VEGF mRNA LNP 55 partially restores a healthy immune landscape in the blood and placenta. a–**c**, Immunophenotyping was performed to evaluate differences in the proportion of immune cell populations in the (**a**) blood, (**b**) spleen, and (**c**) placenta in inflammation-induced pre-eclampsia following administration of the VEGF mRNA LNP 55 therapeutic. The proportion of immune cells are reported as mean ± s.e.m. ($n = 8$ biological replicates). Ordinary two-sided, one-way (**a**–**b**) or nested two-sided, one-way (**c**) ANOVAs with post hoc Student's *t* tests using the Holm-Šídák correction for multiple comparisons were used to compare responses across treatment groups.

nature portfolio

Corresponding author(s): Michael J. Mitchell

Last updated by author(s): Sep 26, 2024

Reporting Summary

Nature Portfolio wishes to improve the reproducibility of the work that we publish. This form provides structure for consistency and transparency in reporting. For further information on Nature Portfolio policies, see our Editorial Policies and the Editorial Policy Checklist.

Statistics

For all statistical analyses, confirm that the following items are present in the figure legend, table legend, main text, or Methods section.

n/a	Confirmed	
☐	☒	The exact sample size (*n*) for each experimental group/condition, given as a discrete number and unit of measurement
☐	☒	A statement on whether measurements were taken from distinct samples or whether the same sample was measured repeatedly
☐	☒	The statistical test(s) used AND whether they are one- or two-sided *Only common tests should be described solely by name; describe more complex techniques in the Methods section.*
☐	☒	A description of all covariates tested
☐	☒	A description of any assumptions or corrections, such as tests of normality and adjustment for multiple comparisons
☐	☒	A full description of the statistical parameters including central tendency (e.g. means) or other basic estimates (e.g. regression coefficient) AND variation (e.g. standard deviation) or associated estimates of uncertainty (e.g. confidence intervals)
☐	☒	For null hypothesis testing, the test statistic (e.g. *F*, *t*, *r*) with confidence intervals, effect sizes, degrees of freedom and *P* value noted *Give P values as exact values whenever suitable.*
☒	☐	For Bayesian analysis, information on the choice of priors and Markov chain Monte Carlo settings
☒	☐	For hierarchical and complex designs, identification of the appropriate level for tests and full reporting of outcomes
☒	☐	Estimates of effect sizes (e.g. Cohen's *d*, Pearson's *r*), indicating how they were calculated

Our web collection on statistics for biologists contains articles on many of the points above.

Software and code

Policy information about availability of computer code

Data collection	Perkin Elmer Living Image 4.7.3 for In Vivo Imaging System (IVIS) BD FACSDiva v9.0 for BD LSR II and LSRFortessa flow cytometers Luminex InCyte 4.5 for Guava easyCyte flow cytometer Leica Application Suite X (LAS X Office 1.4.6) for Leica Stellaris 5 confocal scanning light microscope
Data analysis	ImageJ2 Version 2.14.0/1.5f FlowJo Version 10.10.0 RStudio Version 2024.09.0+375 GraphPad Prism Version 10.3.1 (464)

For manuscripts utilizing custom algorithms or software that are central to the research but not yet described in published literature, software must be made available to editors and reviewers. We strongly encourage code deposition in a community repository (e.g. GitHub). See the Nature Portfolio guidelines for submitting code & software for further information.

Data

Policy information about availability of data

All manuscripts must include a data availability statement. This statement should provide the following information, where applicable:

- Accession codes, unique identifiers, or web links for publicly available datasets
- A description of any restrictions on data availability
- For clinical datasets or third party data, please ensure that the statement adheres to our policy

Demultiplexed next-generation sequencing data from b-DNA LNP screening are available at https://upenn.box.com/v/VEGF-LNPs-pre-eclampsia. Source code 1 for read extraction and tabulation is provided with this paper. Source code 2 for data transformation/normalization is provided with this paper. All other source data are provided with this paper.

Human research participants

Policy information about studies involving human research participants and Sex and Gender in Research.

Reporting on sex and gender	N/A
Population characteristics	N/A
Recruitment	N/A
Ethics oversight	N/A

Note that full information on the approval of the study protocol must also be provided in the manuscript.

Field-specific reporting

Please select the one below that is the best fit for your research. If you are not sure, read the appropriate sections before making your selection.

☒ Life sciences ☐ Behavioural & social sciences ☐ Ecological, evolutionary & environmental sciences

For a reference copy of the document with all sections, see nature.com/documents/nr-reporting-summary-flat.pdf

Life sciences study design

All studies must disclose on these points even when the disclosure is negative.

Sample size	All sample sizes had at least n = 3 biological replicates and no statistical methods were used to predetermine sample size.
Data exclusions	No data was excluded from analyses.
Replication	For in vitro assays, experiments were replicated with at least n = 3 independent biological replicates each with multiple technical replicates. An independent biological replicate was plated from a unique cell subculture/passage and a technical replicate was considered one well of plated cells. For in vivo assays, experiments were replicated with at least n = 3 biological replicates/mice. All attempts at replication were successful.
Randomization	Mice were randomly allocated into experimental groups.
Blinding	Investigators were not blinded during outcome assessment or data analysis. Blinding was not relevant to the study as no subjective data collection or scoring was required.

Reporting for specific materials, systems and methods

We require information from authors about some types of materials, experimental systems and methods used in many studies. Here, indicate whether each material, system or method listed is relevant to your study. If you are not sure if a list item applies to your research, read the appropriate section before selecting a response.

Materials & experimental systems

n/a	Involved in the study
☐	☒ Antibodies
☐	☒ Eukaryotic cell lines
☒	☐ Palaeontology and archaeology
☐	☒ Animals and other organisms
☒	☐ Clinical data
☒	☐ Dual use research of concern

Methods

n/a	Involved in the study
☒	☐ ChIP-seq
☐	☒ Flow cytometry
☒	☐ MRI-based neuroimaging

Antibodies

Antibodies used

Brilliant Violet 421 anti-mouse CD45, BioLegend Cat. #103134 Clone 30-F11
Brilliant Violet 711 anti-mouse CD19, BioLegend Cat. #115555 Clone 6D5
FITC anti-mouse CD3, BioLegend Cat. #100204 Clone 17A2
PE anti-mouse CD11c, BioLegend Cat. #117308 Clone N418
PE/Cyanine7 anti-mouse/human CD11b, BioLegend Cat. #101216 Clone M1/70
FITC anti-mouse CD31, BioLegend Cat. #102506 Clone MEC13.3
PE anti-mouse Cytokeratin 7, Novus Biologicals Cat. #NBP2-47940PE
Recombinant anti-mouse/rat/human cytokeratin 7, Abcam Cat. #ab181598 Clone EPR17078
PE anti-rabbit IgG, BioLegend Cat. #406421 Clone Poly4064
Recombinant anti-mouse endomucin, R&D Systems Cat. #AF4666 Clone Q9R0H2
FITC anti-goat IgG, Abcam Cat. #ab6881
Spark 387 anti-mouse CD8, BioLegend Cat. #100798 Clone 53-6.7
Brilliant Violet 421 anti-mouse CD4, BioLegend Cat. #100443 Clone GK1.5
PerCP anti-mouse CD45, BioLegend Cat. #103130 Clone 30-F11
PE anti-mouse CD25, BioLegend Cat. #101904 Clone 3C7
Alexa Fluor 700 anti-mouse CD11c, BioLegend Cat. #117320 Clone N418
APC anti-mouse CD3, BioLegend Cat. #100236 Clone 17A2

Validation

All primary antibodies were validated by the manufacturer to have reactivity against mouse targets.

Recombinant anti-mouse/rat/human cytokeratin 7: Knock-out (KO) validation was used to confirm antibody specificity by testing the antibody of interest in a cell line or tissue that has been engineered to not express the target protein.

Recombinant anti-mouse endomucin: Detects mouse Endomucin in direct ELISAs and Western blots. In direct ELISAs, less than 5% cross-reactivity with recombinant human Endomucin-2 is observed.

All BioLegend antibodies: Specificity testing of 1-3 target cell types with either single- or multi-color analysis (including positive and negative cell types). Once specificity is confirmed, each new lot must perform with similar intensity to the in-date reference lot. Brightness (MFI) is evaluated from both positive and negative populations.

Eukaryotic cell lines

Policy information about cell lines and Sex and Gender in Research

Cell line source(s)

Hep G2 (HB-8065) cells derived from a male patient with hepatocellular carcinoma were purchased from ATCC.
Jurkat (TIB-152) cells derived from a male patient with acute T cell leukemia were purchased from ATCC.
RAW 264.7 (TIB-71) cells derived from a male mouse with a tumor induced by Abelson murine leukemia virus were purchased from ATCC.
Raji (CCL-86) cells derived from a male patient with lymphoma were purchased from ATCC.
BeWo b30 cells derived from a patient with choriocarcinoma were gifted from Dr. Dan Huh at the University of Pennsylvania with permission of Dr. Alan Schwartz at the University of Washington St. Louis. The original BeWo cell line (CCL-98) was purchased from ATCC.

Authentication

The morphology of all cells was checked at every subculture/passage to ensure they were free from contamination for authentication purposes.

Mycoplasma contamination

All cell lines tested negative for mycoplasma at the University of Pennsylvania's Cell Center.

Commonly misidentified lines
(See ICLAC register)

No commonly misidentified cell lines were used in the study.

Animals and other research organisms

Policy information about studies involving animals; ARRIVE guidelines recommended for reporting animal research, and Sex and Gender in Research

Laboratory animals

Non-pregnant 6–8 week old female C57BL/6 mice and time-dated pregnant female C57BL/6 mice were purchased from Jackson

Laboratory animals	Laboratory (Bar Harbor, ME). Time-dated pregnancies were also achieved by housing four C57BL/6 females and one C57BL/6 male all at least 8–10 weeks of age together in one cage overnight and separating the male the next morning. Consistent with the breeding scheme established by Jackson Laboratory, separation was deemed to be gestational day E0. Pregnancies were confirmed visually on or after gestational day E11 or by measuring weight change. Mice housed in a vivarium with a 12 h light/dark cycle and were provided food and water ad libitum. Vivarium temperature and humidity was maintained between 68–76 F and 30–70%, respectively.
Wild animals	No wild animals were used in the study.
Reporting on sex	Findings only apply to one sex, all studies in the present work utilized female mice.
Field-collected samples	Study did not involve samples collected from the field.
Ethics oversight	All animal use was in accordance with the guidelines and approval from the University of Pennsylvania's Institutional Animal Care and Use Committee (IACUC, protocol #806540).

Note that full information on the approval of the study protocol must also be provided in the manuscript.

Flow Cytometry

Plots

Confirm that:

☒ The axis labels state the marker and fluorochrome used (e.g. CD4-FITC).

☒ The axis scales are clearly visible. Include numbers along axes only for bottom left plot of group (a 'group' is an analysis of identical markers).

☒ All plots are contour plots with outliers or pseudocolor plots.

☒ A numerical value for number of cells or percentage (with statistics) is provided.

Methodology

Sample preparation	Following dissection, spleens and placentas were collected into 2 mL of dH2O and placed on ice. Organs were passed through 100 µm cell strainers to generate cell suspensions. Placenta cell suspensions were treated with 1% (v/v) 2000 U/mL DNase I and 10% (v/v) 10X DNase I buffer for 30 min at room temperature. ACK lysis buffer was added to blood, spleen, and placenta cell suspensions for 5 min, cells were spun at 500 g for 5 min, and the supernatant was removed. ACK lysis was repeated until red blood cells were removed, and the resulting pellet was resuspended in 1X PBS with 2 mM EDTA. 0.5 µL of TruStain FcX PLUS (anti-mouse CD16/32) antibody was added to each sample for 10 min at 4 oC. Samples were then stained for cell surface markers, washed, and if applicable, fixed, permeabilized, and stained for intracellular markers.
Instrument	BD LSR II flow cytometer equipped with violet, blue, green, and red lasers BD LSRFortessa flow cytometer equipped with ultraviolet, violet, blue, yellow/green, and red lasers Guava easyCyte flow cytometer equipped with blue, green, and red lasers
Software	BD FACSDiva software and Luminex InCyte software were used to acquire flow cytometry data. FlowJo was used to analyze flow cytometry data.
Cell population abundance	For in vitro samples, at least 10,000 events corresponding to singlets were acquired for all experimental samples. For mouse-derived samples, at least 50,000 events corresponding to singlets were acquired for all spleen and placenta experimental samples and at least 10,000 events corresponding to singlets were acquired for blood experimental samples.
Gating strategy	Thresholds for positivity were determined using fluorescence-minus-one (FMO) controls with representative gating schemes found in the Supplementary Information.

☒ Tick this box to confirm that a figure exemplifying the gating strategy is provided in the Supplementary Information.